A Study on the effect of focused laser beam on the fluorescence of ZnO nanowires

Hew Kai Ming A0098123E

Supervised by Prof. Sow Chorng Haur

Acknowlegdement

First, I would like to thank my supervisor, Prof. Sow Chorng Haur for offering me challenging and interesting projects since the period of my UROPS study. Not to forget also my mentor, Mr. Lim Kim Yong who has guided me all the time since the first day I entered the NUS Nanomaterials Laboratory. Without their guidance and suggestions, this thesis may not achieve practical yet satisfying targets and more likely may deviate from the initial motivation. I appreciate all advice and discussions from these professionals especially in the aspect of refining the job scope of this study.

I would also like to extend my appreciation to Dr. Zheng Minrui, Dr. Lu Junpeng and Dr. Sharon Lim Xiao Dai for their practical assistance in handling a series of equipments like FM, Raman Microscope and Focused Laser Beam System. In particular, special thanks to Dr. Zheng for passing down his experience in the study of ZnO nano-structures.

Furthermore, my gratitude extends to all my batch mates who are working in the same laboratory under the same supervisor. Thanks to a number of fruitful discussions with them, I have been able to look at my study in a different angle. I would like to especially express my gratitude to Mr. Hu Zhen Liang for sharing his experience in the the growth of GeS to help me understanding the causes of a similar problem in the synthesis of ZnO nanowires.

Last but not least, I would like to thank my family members who have been financially and mentally supporting me throughout my whole undergraduate studies. As a result of their encouragement and concern, I have been able to face all kinds of difficulties and finally complete my education.

Abbreviations

ZnO → Zinc Oxide

NWs → Nanowires

PVD → Physical Vapor Deposition

CVD → Chemical Vapor Deposition

FM → Fluorescence Microscopy

PL → Photoluminescence

XPS → X-ray Photo-electron Spectroscopy

Laser → Light Amplification by Stimulated Emission of Radiation

SEM → Scanning electron microscopy

TEM → Transmission electron microsopy

EDX → Energy-Dispersive X-ray Spectroscopy

LED → Light Emitting Device

UV → Ultraviolet

DOS → Density of state

Content

Chapter 1

1.1 Abstract 9

1.2 Introduction 9

- General remark on ZnO nanostructures
- Basic structure(s) of ZnO
- Typical ZnO nanostructures
- Fluorescence property and a brief review on their underlying principles

1.3 Motivation 16

Chapter 2

Experimental 19

- 2.1 Synthesis 19
  - 2.1.1 Pre-synthesis preparations
  - 2.1.2 PVD
  - 2.1.3 CVD
  - 2.1.4 Adjustable parameters during synthesis

- 2.2 Measurements 23
  - 2.2.1 Extraction by dry transfer
  - 2.2.2 FM
  - 2.2.3 PL
  - 2.2.4 XPS
  - 2.2.5 Raman

- 2.2.6 Laser Pruning
- 2.2.7 SEM
- 2.2.8 EDX
- 2.2.9 TEM

Chapter 3

Results and discussions 34

- 3.1 Control of the resulted emission 34
  - 3.1.1 Manipulation of the mass ratio of the components of the precursor
  - 3.1.2 Position control
  - 3.1.3 Oxygen

- 3.2 TEM and XPS study on Green- and Brown-fluorescence specimen 46

- 3.3 Laser Modification 49
  - 3.3.1 Disintegration by laser beam in brown and green samples
  - 3.3.2 Brown-green fluorescence alteration by laser beam

Conclusion(s) 63

Future Works 64

Appendices 65

All Figures

Fig 1 Table of the functionalities of nanowires of different materials

Fig 2 Different Crystal Structures of ZnO

Fig 3 a) 4-digit Miller-Bravais indices for planes in a hexagonal lattice system

b) Selected examples for the directions in the hexagonal system using 3-digit indices

Fig 4 FESEM images of different ZnO nano-structures

Fig 5 Different types of point defects which are commonly discussed in ZnO nanostructures

Fig 6 Different fluorescence as seen by naked eyes under UV excitation

Fig 7 Proposed mechanisms for different emissions of ZnO nanostructures

Fig 8 Achievable emissions of ZnO NWs under UV excitation (330~380nm)

Fig 9 Change of PL spectrum (325nm excitation) along an as-prepared ZnO NWs sample

Fig 10 Laser pruning done on different nano-materials

Fig 11 (a) Schematic diagram of sputtering machine

(b) Photograph of the setup of the sputtering system

Fig 12 (a) Schematic diagram of CVD

(b) Photograph of the furnace used for CVD

Fig 13 Schematic diagram of dry transfer technique

Fig 14 Extracting the nanowires out from as-prepared sample

Fig 15 (a) Schematic diagram of fluorescence microscopy

(b) Photograph of the FM

Fig 16 Transmission profile of dichromatic mirror as a function of wavelength

Fig 17 Basic principle of PL

Fig 18 Schematic diagram of the basic components of XPS

Fig 19 Schematic diagram of Raman Scattering

Fig 20 (a) Schematic diagram of focused laser beam system

(b) Photograph of the focused laser beam setup

Fig 21 (i) Schematic diagram of field emission

(ii) Schematic diagram of SEM

Fig 22 Schematic diagram of different SEM signals.

Fig 23 (i) Schematic diagram of TEM

(ii) Photograph of TEM in EM lab of NUS chemistry department

Fig 24 Schematic diagram of EDX

Fig 25 FM images of bulk NWs surface (first row), extracted individual NW (second row) and their corresponding PL spectrum

Fig 26 A typical image processed by Google Sketch-up

Fig 27 A rough estimation of the proportion of different colors from nanowires at one spot

Fig 28 Proposed mechanisms for different emissions of ZnO nanostructures observed in the laboratory

Fig 29 Temperature profile inside the CVD furnace

Fig 30 A typical PL profile of a long sample

Fig 31 SEM images of a typical long sample

Fig 32 Schematic illustration of the diffusion of source materials through the gas flow boundary layer

Fig 33 SEM image taken on sample synthesized using short samples placed at different spots

Fig 34 Fluorescence of both bulks NWs surface and extracted nanowires grown under different diffusion and temperature conditions

Fig 35 FM images of two kinds of green sample

Fig 36 FM images of both bulk NWs surface and individual nanowire before and after oxygen annealing in atmosphere

Fig 37 TEM results of green- and brown-fluorescence samples

Fig 38 XPS spectra of green-fluorescence ZnO NWs (Sample A) and brown-fluorescence ZnO NWs (Sample E)

Fig 39 Laser modification on a brown ZnO NWs sample

Fig 40 Laser modification on a green ZnO NWs sample

Fig 41 Drawing Porygon using focused laser beam

Fig 42 Writing Secret Message on the ZnO NWs sample

Fig 43 FM image of the laser-modified sample vs unmodified sample

Fig 44 FM images of an as-prepared sample after laser modification with different powers

Fig 45 PL spectra from regions after laser modification with different powers

Fig 46 Raman spectra after laser modification with different powers

Fig 47 Typical EDX spectrum and elemental composition at region modified by laser with different powers

Fig 48 EDX mapping of different elements

Fig 49 SEM images of regions modified by laser beam with different powers

Fig 50 Top: Plots of the atomic percentage of Zn, O and C versus the power of focused laser beam,

Bottom: A table of the data points

1.1 Abstract

Grown by chemical vapor deposition, ZnO nanowires can exhibit a wide range of fluorescence under UV excitation from red to violet depending on the synthesis parameters. In this study, schemes to produce nanowires of different emission wavelengths were investigated. Characterization on both the emissions from the sample surface and the individual nanowire was also conducted with the use of techniques such as fluorescence microscopy (FM), photoluminescence spectroscopy (PL), X-ray photo-electron spectroscopy (XPS). In addition to have a better understanding on the principle behind the fluorescence, the focus of this study will mainly be the way and possible causes of laser modification on the sample surface as well as individual nanowire.

Chapter 1

1.1 Introduction

General remark on ZnO nanostructures

For decades, people has been studying ZnO materials as well as its nano-structures, mainly because of its large exciton binding energy (~60 meV) and wide band gap (~3.3 eV) which is comparable to that of GaN (~3.4 eV), under room temperature and pressure.[1] This shows the potential application of ZnO in optoelectronic devices such as LED (as a substitute of the commonly used GaN), photo-detector and sensor.[2] One can refer to Fig 1 to see the possible ZnO applications. On the other hand, ZnO nanostructures are also able to exhibit a wide range of emissions with different wavelengths, possibly as a result of different defect-related levels.[3] This kind of fluorescence property under optical excitation has great implication in a variety of sensing applications.

Nanowires	Optical functions	Characteristics
GaN	Nanolaser	Emission wavelength: 370-390 nm Threshold: ~500 mJ/cm^2 Cavity Q factor: 500-1500 Threshold gain: 400-1000 cm^{-1}
	Light-emitting diodes	Emission wavelength: 380-420 nm
ZnO	Nanolaser	Emission wavelength: 370-400 nm Threshold: >70 mJ/cm^2 Cavity Q factor: 1000-1500 Threshold gain: 1000-3000 cm^{-1}
	Frequency converter	Effective second-order susceptibility: 5.5 pm/V
	Solar cell	Energy converting efficiency: 3.5%
	Photodetector	UV light detector
SnO_2	Waveguide	Propagation loss: 1-8 dB mm^{-1}
	Evanescent wave optical sensor	Single molecular level detection

Fig 1, Table of the functionalities of nanowires of different materials. Notice the abundance of the possible functionalities of ZnO nanowires as compared to GAN and SnO_2. (Adapted from [4])

Basic structure(s) of ZnO

In nature, there are three types of ZnO crystal structures, namely the wurtzite, zinc blende and rocksalt structure. These structures can be visualized in Fig 2.

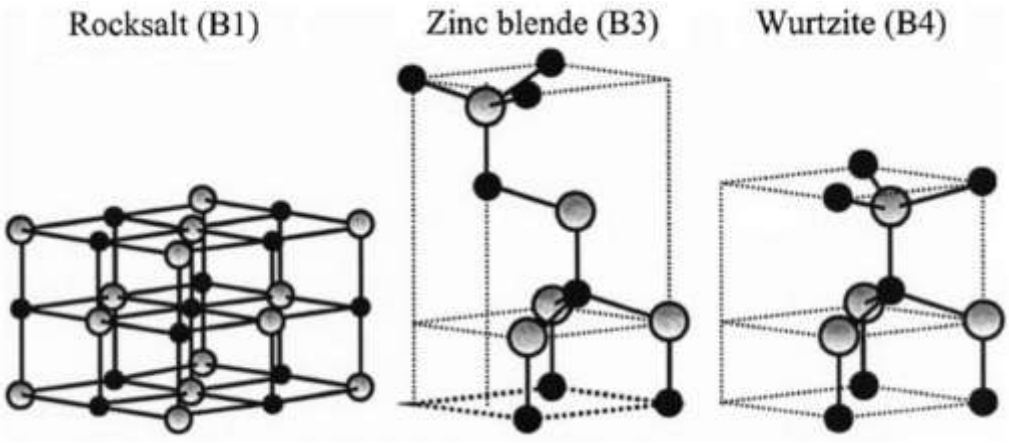

Fig 2, Different Crystal Structures of ZnO.[5]

While zinc blende and rocksalt structures are only found in specific cases, we will only discuss the wurtzite structure, which is the most abundant species among the three. The lattice and basis of wurtzite structure is shown in Fig 3.

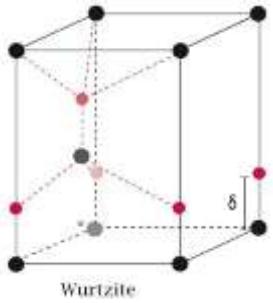

Fig 3, Wurtzite structure containing two different atoms. Notice there is a shift of d along the c-axis between the bases of the two atoms. Thus, the basis of the first element are $(0\ 0\ 0)$ and $\left(\frac{2a}{3}\frac{a}{3}\frac{c}{2}\right)$, while for the second element are $(0\ 0\ \delta)$ and $\left(\frac{2a}{3}\frac{a}{3}\frac{c}{2}+\delta\right)$.

Hexagonal lattice:

From a number of studies [6, 7], ZnO NWs usually exhibit a shape of hexagonal wire. Thus, it is sometimes convenient to discuss the lattice structure based on the hexagonal lattice system.

Due to symmetry of hexagonal structure, a four-axes (a_1, a_2, a_3, c) coordinate system is utilized, resulting in a 4-digit Miller-Bravais indices (*hkil*). The additional i-index is defined by the following relation:

$$h + k + i = 0$$

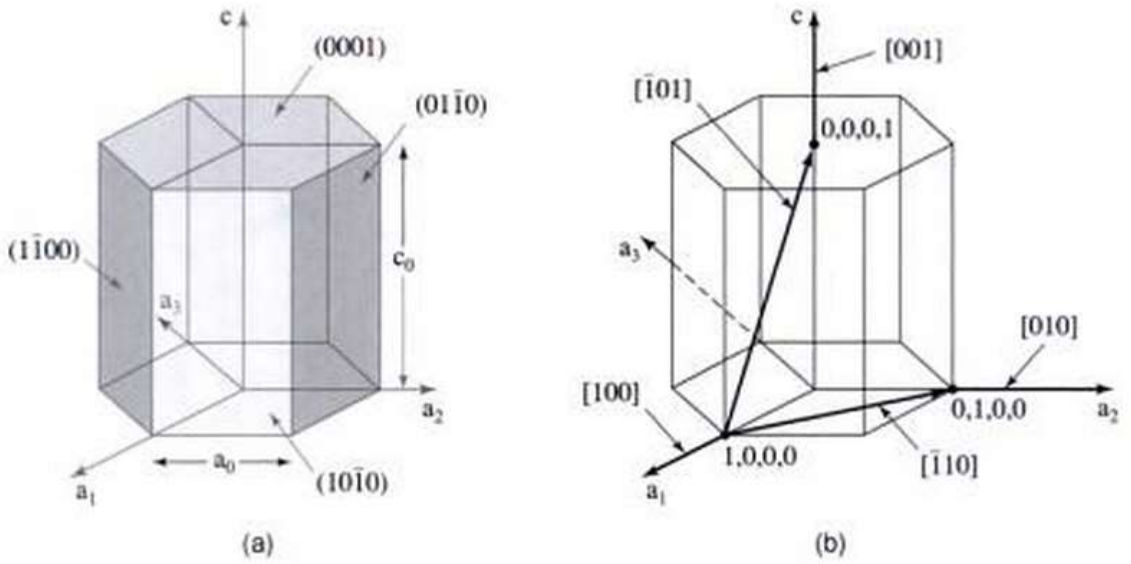

Fig 4, a) 4-digit Miller-Bravais indices for planes in a hexagonal lattice system, (b) Selected examples for the directions in the hexagonal system using 3-digit indices. The coordinate intercepts are given with commas to separate them.[8]

As shown in Fig 3(a), the top and bottom planes are the basal planes with indices of type [0001]. The indices for the six vertical planes are of type [1-100].

In most cases, the directions in the system are more conveniently expressed by 3-digit indices, as shown in Fig 3(b). For instance, the direction $\frac{1}{3}$[2-1-10] can just simply written as [100] instead.

Typical ZnO nanostructures:

Occasionally 1-D ZnO nano-structures have grabbed attention due to its quantum confinement features. These features lead to a series of unique electrical and optical properties which are potentially useful in developing new generation nano-devices, including short-wavelength nanolasers, field-effect transistors, ultrasensitive nano-sized gas sensors, nano-resonators, transducers, actuators, nano-cantilevers, and field emitters. [6][7][8]

According to the outer appearance, we can classify 1-D nano-structures into nano-rod, nanowire, nano-tube, nano-ring, etc. Some of the SEM images of these nano-structures are shown in Fig 5.

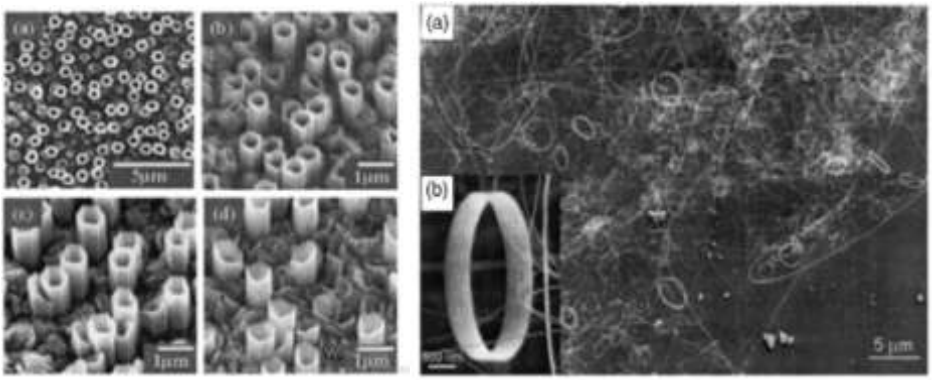

(i) (ii)

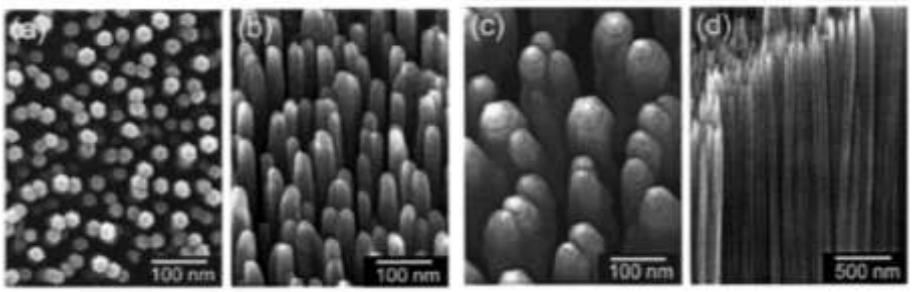

(iii)

Fig 5, FESEM images of (i) ZnO nanotubes, (ii) nanorings, (iii) nanorods.

[Adapted from , (i) B. P. Zhang, N. T. Binh, K. Wakatsuki, Y. Segawa, Y. Yamada, N. Usami, M,, (ii) X. Y. Kong, Y. Ding, R. Yang, and Z. L. Wang, Science 303, 1348 2004, (iii) W. I. Park, D. H. Kim, S.-W. Jung, and G.-C. Yi, Appl. Phys. Lett. 80, 4232 2002.]

In particular, ZnO nanowires exhibit a number of unique optical properties. First, room temperature photoluminescence shows that it has a sharp band edge emission at ~377 nm even at low excitation intensities. With high enough excitation intensity, stimulated emissions at other regions, for instance 440-480nm and 510-580nm, are also observed. Apart from that, defect-related yellow emissions beyond 600nm are seen at a number of occasions.[9]

Fluorescence property and a brief review on their underlying principles:

In principle, a perfect ZnO structure exhibits a single emission, which is as a result of its characteristic excitonic recombination. In actual situation, non-equilibrium processes often happen during the synthesis stage of the ZnO structures, leading to the introduction or formation of a variety of defects such as vacancies[10, 11, 12], anti-sites[13] and interstitials[14], as shown in Fig 6.

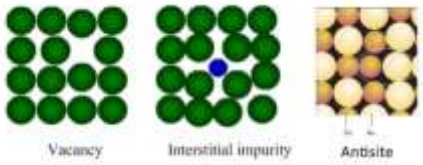

Fig 6, Different types of point defects which are commonly discussed in ZnO nanostructures

This in turn creates additional energy levels in between the band gap, leading to the a series of visible emissions, as shown in Fig 7.

Fig 7, Different fluorescence as seen by naked eyes under UV excitation.

One of the main techniques to study the profiles of the emissions is photoluminescence spectroscopy. Details will be discussed in more depth, along with other techniques used in this project. Here it should be noted that besides to widely accepted exciton peak at about 380 nm (~ 3.3 eV), which corresponds to the excitonic recombination, all other peaks, mainly in the visible region, are still not well understood.

In fact, despite decades of investigations, the identification of these defects, as well as their correlations to different emissions still remains in controversy. In most studies, researchers managed to come out with certain scheme to manipulate the emission. Yet, to explain the origin of those emissions, researchers often analyze the synthesis parameters or perform measurements like XPS, EDX to investigate the possible chemical bonds and the composition. However all those results seldom provide sufficiently direct and solid evidence to correlate an emission to a specific defect. Very often different interpretations on the same raw results which lead to totally different modeling can sound equally sensible. Thus, unless there is any new breakthrough in microscopy which allows us to resolve and image the point defects directly, this field of study is not likely to achieve much satisfactory agreements or conclusions.

In this project, any discussion related to the possible causes of the fluorescence will rely on the model proposed by Professor Zheng Haibo in Fig 8, since this model agrees quite well with our observations so far.

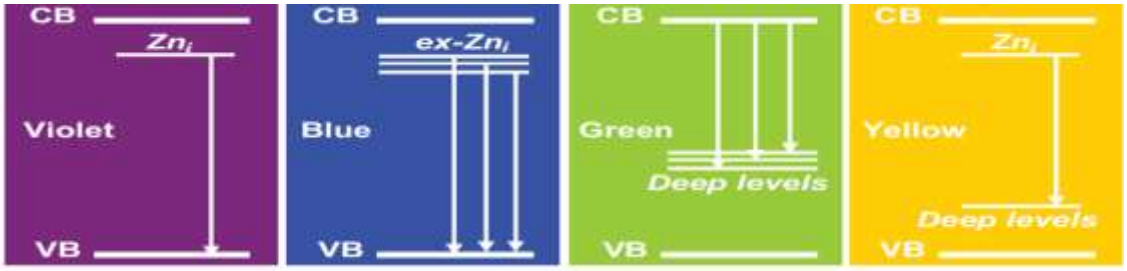

Fig 8, Proposed mechanisms for different emissions of ZnO nanostructures observed in the laboratory.[3]

In Fig 8, CB and VB refer to conduction band and valence band respectively. Zn_i is the Zinc interstitial defect level while the defects corresponding to the deep levels are not known in this model. Transitions between different energy levels will give rise to fluorescence of different colors. The dominant emission will then depend on the concentration of certain defect.

In particular, we will argue that the dominance of yellow or green emission will depend on the density of Zn_i defects which give rise to mainly the shallow energy levels, and also the density of oxygen-related defects and dopant-related defects which give rise to deep levels. The way we verify these proposed mechanisms is mainly based on the assumption that a higher relative concentration of Zn as compared to O_2 will increase the chance of the formation of zinc-related defects and thus DOS of Zn-related defect levels. However, for deep levels, the situation is complicated since both oxygen and dopant like carbon can contribute. Especially when we do not intentionally dope the specimen, we are often unable to have a good control on the amount of dopant.

Nevertheless, the actual principles behind these fluorescence are very complicated. Therefore, in this particular project we will focus more on how to modify the emission of as prepared sample optically instead of solving the whole puzzle.

References

[1] W. Park, G. Yi, Adv. Matter. 2004, 16, 87.

[2] Y. Qin, X. Wang, Z. L. Wang, Nature 2008, 451, 809.

[3] Haibo Zeng, “Blue Luminescence of ZnO Nanoparticles Based on Non-Equilibrium Process: Defects Origins and Emission Controls”, Advanced Functional Materials, 20, pg. 561-572, (2010)

[4] Peter J. Pauzauskie and Peidong Yang, “Nanowires Photonics”, Materials Today, Vol 9, NO. 10, Oct 2006.

[5] U. Ozgur, Ya. I. Alivov, C. Liu, A. Teke, M. A. Reshchikov, S. Dogan, V. Avrutin, S.-J. Cho, and H. Morkoc, “A comprehensive review of ZnO materials and devices, Journal of Applied Physics 98, (2005)

[6] Manpreet Singh, Sheng Song and Jong-in Hahm, “Unique temporal and spatial biomolecular emission profile on individual zinc oxide nanorods”, Nanoscale, 2014, 6, 308.

[7] Ivana LJ and Phillip Ahrenkiel, “Microstructural Analysis and the Multicolor UV/Violet/Blue/Green/Yellow PL Observed from the Synthesized ZnO Nano-leaves and Nano-rods”, METALLURGICAL AND MATERIALS TRANSACTIONS A, VOLUME 46A, AUGUST 2015-3679.

[8] Rolf E. Hummel, “Understanding Materials Science: History, Properties, Applications, Second Edition”, Springer Science and Business Media, (2004)

[9] Zhong Lin Wang, “Nanostructures of zinc oxide”, Mater. Today 7, 26, (2004).

[10] Zhong Lin Wang, “Zinc oxide nanostructures: growth, properties and applications”, Published 11 June 2004, IOP Publishing Ltd, Journal of Physics: Condensed Matter, Volume 16, Number 25

[11] DP Norton, LC Tien, Y Kwon, BS Kang, “Nanowires growth and devices”, Materials Science and Engineering: R: Reports, Volume 47, Issues 1–2, 20 December 2004, Pages 1–47

[12]R. Könenkamp, Robert C. and C. Schlegel, “Vertical nanowire light-emitting diode”, Appl. Phys. Lett. 85, 6004 (2004).

[13] K. Vanheusden, W. L. Warren, C. H. Seager, D. R. Tallant, J. A. Voigt1 and B. E. Gnade, “Mechanisms behind green photoluminescence in ZnO phosphor powders”, J. Appl. Phys. 79, 7983 (1996)

[14] Hong Seong Kang, Jeong Seok Kang, Jae Won Kim and Sang Yeol Lee, “Annealing effect on the property of ultraviolet and green emissions of ZnO thin films”, J. Appl. Phys. 95, 1246 (2004)

[15] S. A. Studenikin, Nickolay Golego and Michael Cocivera, “Fabrication of green and orange photoluminescent, undoped ZnO films using spray pyrolysis”, J. Appl. Phys. 84, 2287 (1998)

[16] B. Lin, Z. Fu, and Y. Jia, Appl. Phys. Lett. 79, 943, (2001).

[17] N. O. Korsunska, L. V. Borkovska, B. M. Bulakh, L. Yu. Khomenkova, V. I. Kushnirenko, and I. V. Markevich, J. Lumin. 102–103, 733 (2003).

1.2 Motivation

From previous study, it was found that without intentionally doping, ZnO NWs samples can exhibit a wide range of fluorescence under the same excitation. As shown in Fig 9, the fluorescence along the as-grown sample changes and this can be achieved by manipulation the synthesis parameters. PL spectra in Fig 10 also prove that there is a shift of yellow-dominance to green-dominance in the fluorescence of the sample when we move from region closer to the precursor to region further away from the precursor. This fact is attractive because it hints the possibility of using a single production line to produce samples of different emissive properties.

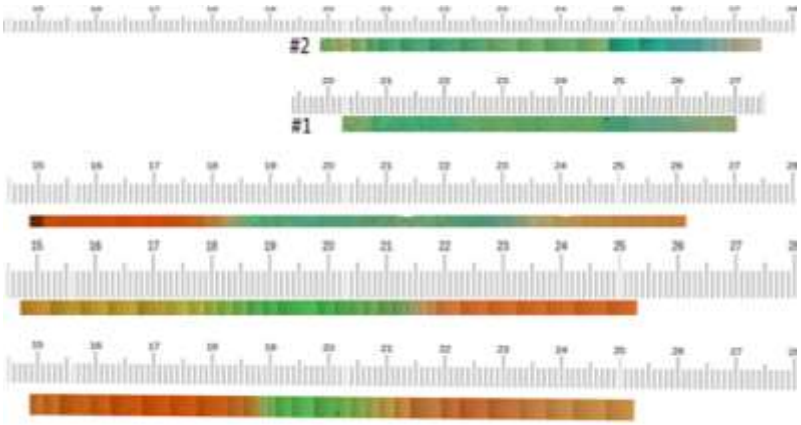

Fig 9, Achievable emissions of ZnO NWs under UV excitation (330~380nm).

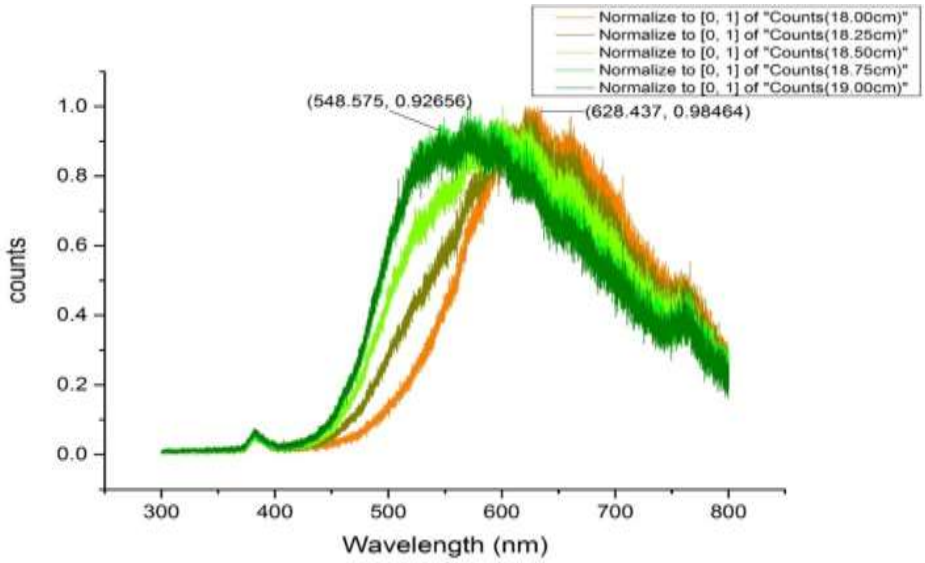

Fig 10, Change of PL spectrum (325nm excitation) along an as-prepared ZnO NWs sample.

With this in mind, the next thing that comes naturally into the room of discussions is the underlying causes of those different kinds of fluorescence. However, from the introduction we have known that

this field of study still remains in controversy although a bunch of possible models have been proposed. In this project, we attempt to develop a slightly better understanding based on the analysis of our results.

Moreover, it is always good to have additional tool to modify the as-prepared sample. Thus, this project tries to focus only on how the focused laser beam will alter the as-prepared fluorescent ZnO NWs samples, as well as the possible cause(s) for the alteration(s). The main reason of employing the focused laser beam as our main research focus is because it is very facile and localized in performing modification. This allows the possibility of conducting on demand laser-induced photo-chemical reactions on our sample to improve its functionalities. Fig 11 shows a series of nano-materials successfully modified using focused laser beam. These successful examples also convince us that laser beam might be a good option.

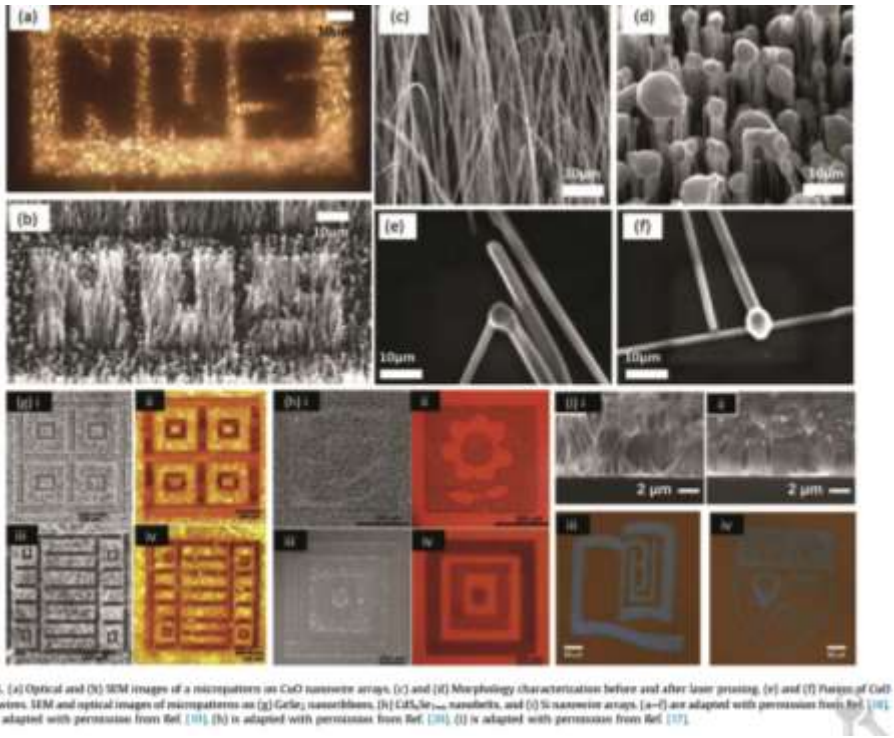

Fig 11, Laser pruning done on different nano-materials. (Adapted from "A Focused Laser Beam: A Useful and Versatile Tool for 1D Nano-materials Research: A Review", Journal of Materials Science & Technology, Volume 31, Issue 6, June 2015, Pages 616–629)

References

[1] "A Focused Laser Beam: A Useful and Versatile Tool for 1D Nano-materials Research: A Review", Journal of Materials Science & Technology, Volume 31, Issue 6, June 2015, Pages 616–629

Chapter 2

Experimental

2.1 Synthesis:

2.1.1 Pre-synthesis preparation

Before undergoing any kinds of deposition, preparations for the precursor and the substrate are conducted. For precursor, Zinc oxide powder (99.99% purity) and graphite powder (20 μm in size) are mixed evenly together by means of grinding. For substrate, the only substrate used in this study is Si (110) wafer. Due to the compatibility with our experimental setup, the silicon wafer is sliced into pieces with a width of approximately 1cm. The length of the substrate depends on the synthesis scheme we employ. The Si substrates are cleaned in three different reagents: acetone, ethanol and distilled water consecutively for 10 minutes respectively, using a ultrasonic cleansing machine. To dry them, the wafers are flushed with nitrogen gas.

2.1.2 Physical Vapor Deposition by Sputtering

The purpose of conducting sputtering is to deposit a nucleation layer onto the substrate, to facilitate the growth of ZnO nanowires. In most cases, this layer requires material which shares similar crystal structure or lattice structure to the underlying substrate and also the material to be grown. In our case, we choose ZnO as our sputtering target.[2]

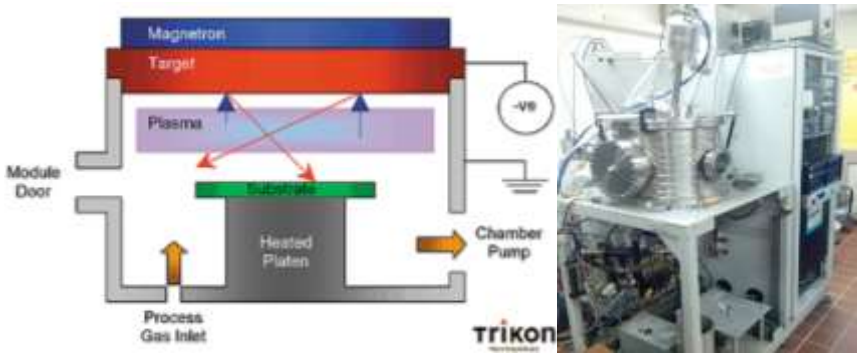

(a) (b)

Fig 12, (a) Schematic diagram of sputtering machine. (Adapted from "Silicon VLSI Technology: Fundamentals, Practice and Models"), (b) Photograph of the setup of the sputtering system.

The sputtering process can be clearly understood by referring to the schematic diagram in Fig 12. Before beginning the sputtering, clean Si wafers are inserted into the chamber of the RF magnetron

sputtering machine. Then, the chamber is pumped down to a pressure of a few 10^{-7} torr and this process takes several hours. When the optimum pressure has been reached, the chamber is heated to approximately 500 °C. After the stabilization of the temperature, Argon gas (99% purity) is introduced. Next, under 100 W RF power, Argon plasma is generated. Directed by the magnetic field, the energetic particles (Ar^+ or Ar radicals) will hit against the sputtering target, kicking out the ZnO atoms, causing them to fall and land onto the Si wafers. This process will last precisely for 25 minutes and result in a ZnO seed layer with a thickness of approximately 200 nm.

2.1.3 Zinc-rich Chemical Vapor Deposition

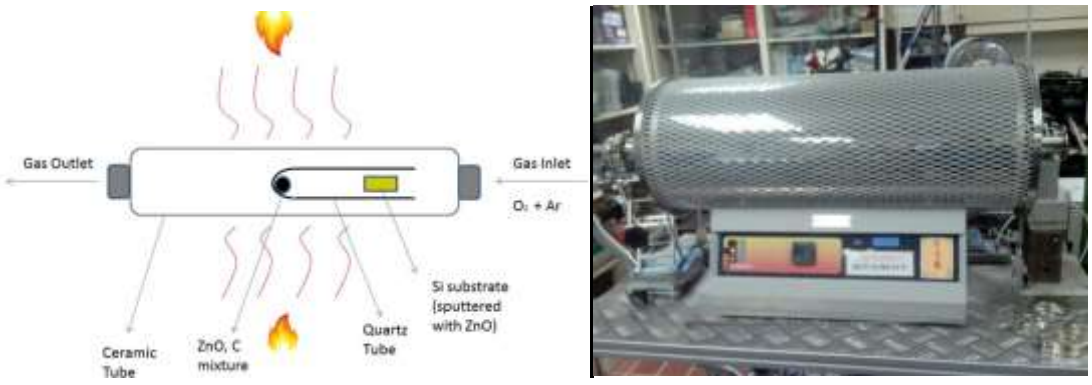

(a) **(b)**

Fig 13, (a) Schematic diagram of CVD, (b) Photograph of the furnace used for CVD

The ZnO nanowires sample is grown by means of LPCVD (low pressure chemical vapor deposition). Referring to schematic diagram in Fig 13, the ZnO in the well-mixed precursor is first reduced by carbon to Zn, and then transported by the carrier gas (99.5% Argon + 0.5% oxygen) to the substrate. There, the Zn reacts with the oxygen to form ZnO again. The related chemical reactions are shown below.[3]

$$ZnO_{(s)} + 2C_{(s)} \longrightarrow Zn_{(g)} + CO_{(g)}$$

$$Zn_{(g)} + \frac{1}{2}O_{2}{}_{(g)} \longrightarrow ZnO_{(s)} \qquad \text{(1) \& (2)}$$

The reason of reducing ZnO and then re-oxidizing is due to the extremely high boiling point of ZnO (~1975 °C). Since Zn has a far lower boiling point of ~905 °C, this allows us to synthesize our sample in a more energy-saving and economic way, because only very specific furnace is able to sustain such high temperature.

Notice the above two chemical reactions have over-simplified the processes involved. More realistically, the Zn vapor will first condense on the substrate, forming droplets. The droplets, whether further react with oxygen to form oxides or not, will define the size of the nanowires and the direction of growth.[4] When more Zn vapor arrives, further oxidation will increase the concentration of oxygen within these droplets, and ZnO will then deposit at the interface between the droplet and the substrate.[5] Led by the droplet, the growth directions of the nanowires usually include [01-10], [2-1-10] and the c-axis (refer to the hexagonal lattice system), because facets with higher surface energies often possess smaller area and vice versa, resulting in higher growth rate in these directions. While the epitaxial orientation of the nanowires is determined by the substrate, the alignment of the nanowires is not well ordered because the uniformity of the sputtered ZnO seed layer is not sufficiently high.

Another unique feature from this synthesis process is the use of single-opening quartz. This is quite different from the usual straight through gas flow manner, where the carrier gas enters the gas inlet, reaches the precursor first, followed by the substrate, and in the end exits through the gas outlet. In our study, the sequence is slightly different: the carrier gas enters the gas inlet, reaches the opening of the quartz tube, passes by the substrate, reaches the precursor, then the gas is reflected upon hitting against the tube wall and moving in the direction towards the substrate while carrying along the reduced Zn. As a result of the change of gas flow direction at the other end of the quartz tube, there exists gas flows of opposite directions within the quartz tube. This results in a relatively slower resultant gas flow within the quartz tube, as compared to the case of commonly-used straight through mechanism. This allows the substrate to interact with Zn for a longer duration, leading to the formation of zinc-rich sample.

2.1.4 Synthesis parameters

1) Composition of the precursor: In particular, the mass ratio between ZnO powder and graphite powder. The former will determine the mass flow of Zn on the substrate, while the latter is believed to affect the formation of carbide compounds.
2) Temperature: More precisely, the set temperature or the highest possible temperature. By setting a different value, the entire temperature profile inside the furnace will change accordingly.
3) Position: This parameter can be further split into the position of the quartz tube and the position of the substrate within the quartz tube.
    - Position of the quartz tube inside the furnace: Changing this will alter the temperature at the substrate region without significantly affecting the diffusion rate of Zn flow from the source region.
    - Position of the substrate in the quartz tube: Changing this will alter both the diffusion rate and temperature.

4) Composition of the carrier gas: The Zn particles reaching the substrate must be re-oxidized to form ZnO. This leads to the importance of oxygen concentration of the carrier gas in affecting the surface reaction rate.
5) Pressure: From fluid dynamics, it is known that pressure will also dictate the concentration of gas elements in the system. In this study, this parameter is strictly kept as constant to avoid complexity.

References

[1] J. D. Plummer, M. D. Deal, and P. B. Griffin, "Silicon VLSI Technology: Fundamentals, Practice and Models", 2000 by Prentice Hall, Upper Saddle River NJ

[2] Lori E. Greene, Matt Law, Dawud H. Tan, Max Montano, Josh Goldberger, Gabor Samorjai, and Peidong Yang General Route to Vertical ZnO Nanowire Arrays Using Textured ZnO Seeds, Nano Letters Vol 5, NO. 7, pg 1231-1236, (2005)

[3] Bin Xiang, Pengwei Wang, Xingzheng Zhang, Shadi. A. Dayeh, David P. R. Aplin, Cesare Soci, Dapeng Yu, Deli Wang, Rational Synthesis of p-Type Zinc Oxide Nanowire Arrays Using Simple Chemical Vapor Deposition, Nano Letters Vol 7, No. 2, pg 323 - 328, (2007)

[4] Zhong Lin Wang, "Zinc oxide nanostructures: growth, properties and applications", J. Phys. Condens. Matter 16 (2004) R829–R858

[5] B. D. Yao, Y. F. Chan, and N. Wang, "Formation of ZnO nanostructures by a simple way of thermal evaporation", Applied Physics Letters 81, 757 (2002).

2.2 Measurements and Techniques

This section will introduce how we make use of different techniques in order to characterize and modify our sample.

2.2.1 Nanowires extraction by dry transfer technique

A very interesting phenomenon in many similar studies of fluorescence of ZnO nanowires is that almost everybody only cares about the property of bulk sample. It is true that there have been already plenty of works to be done on bulk sample, but then we can only observe the behavior of the sample surface.

To study in more details, we would like to extract the individual nanowire from the bulk sample to further measure its fluorescence.

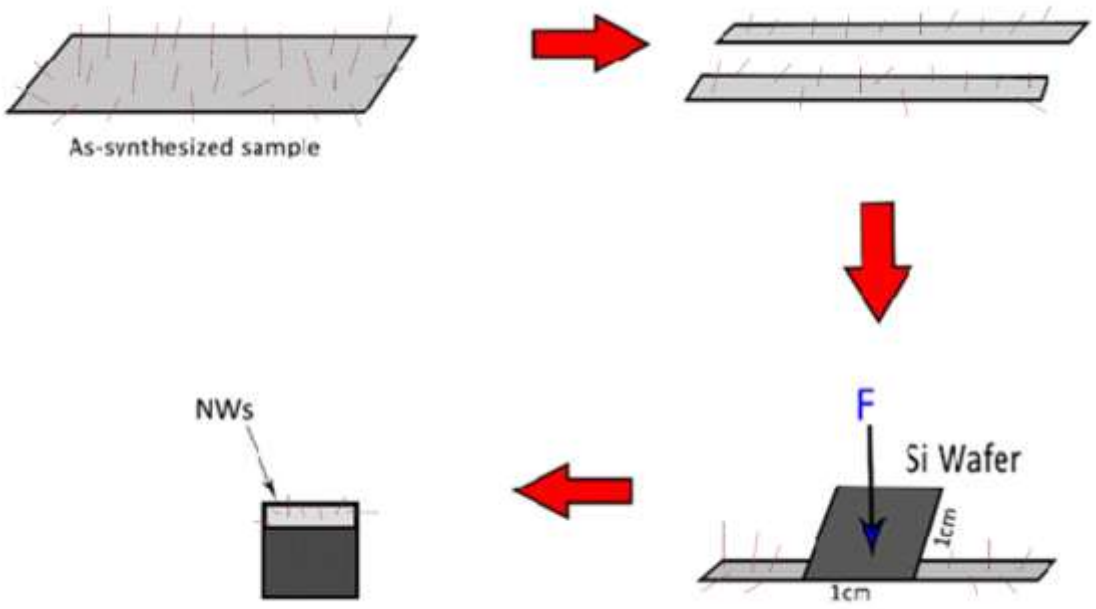

Fig 14, Schematic diagram of dry transfer technique

As shown in Fig 14, the method is quite simple because what needs to do is simply tapping the as-synthesized sample with a piece of clean Si wafer. By chance, some of the nanowires will be transferred onto the Si wafer. Notice the as-grown sample was first sliced into two because we decide to reserve the other half to perform other non-destructive measurements

With this, we can do a series of measurements regarding the emission of the nanowires and make a comparison study between the bulk sample and its individual nanowire.

2.2.2 Fluorescence Microscopy (FM)

Fluorescence microscopy in general refers to technique that uses fluorescence to generate an image. The light beam from the light source is illuminated on the specimen to excite the material, causing it to emit light of longer wavelengths (energy loss due to vibration, etc).

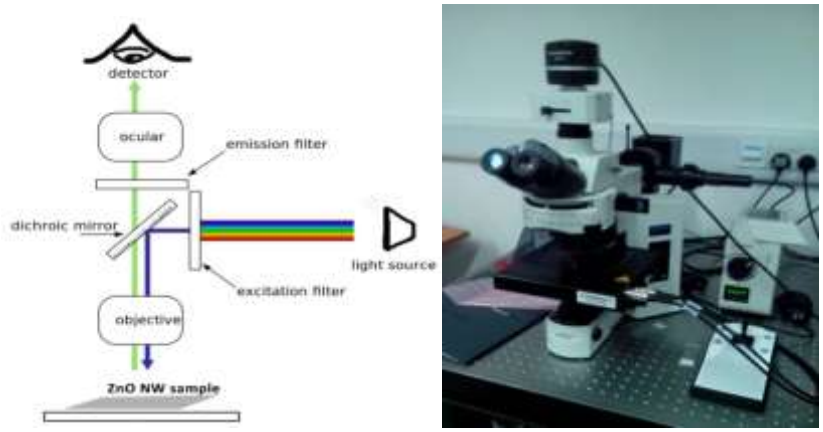

(a) (b)

Fig 15, (a) Schematic diagram of fluorescence microscopy, (b) Photograph of the FM

As shown in Fig 15, the emission from the specimen propagates in all directions and a considerable amount of it, together with the reflected excitation light beam, will reach the dichromatic filter. Referring to the below sample transmission profile, one can observe the dichromatic mirror is designed in such a way the transmission percentages are almost zero between the range of the excitation wavelengths. In this way, only the emission from the specimen can propagate further while the reflected excitation beam is filtered. Note that due to the steepness of the yellow curve, there will always be some excitation beam of certain wavelengths not captured by the dichromatic mirror. Thus a secondary filter is conducted by the emission filter. The final product after these processes is the image of the specimen due to its underlying emission(s).[1]

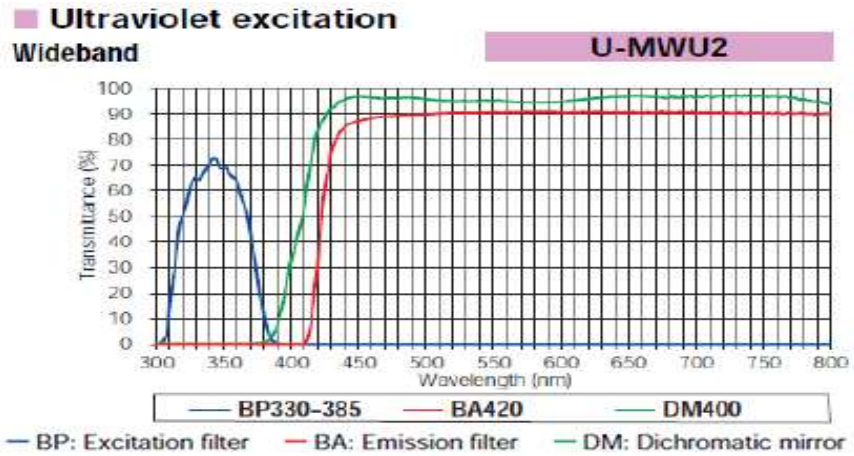

Fig 16, Transmission profile of UV-excitation dichromatic mirror as a function of wavelength

In this study, only UV excitation is utilized. The transmission profile is displayed in Fig 16. The red and green spectra represent the absorption spectra of the emission filter and dichromatic mirror respectively. From the above profile, it is clearly seen that most of the light is filtered and only a short range between 310 to 380 nm is allowed to pass.

2.2.3 Photoluminescence (PL) spectroscopy

Photoluminescence shares similar working principle as fluorescence microscopy, with the exception that the initiation of luminescence is restricted to photo-excitation. The schematic diagram in Fig 17 shows that during the spectroscopy process, photons of a particular wavelength are absorbed and equivalent photons are very rapidly re-emitted. The intensities as a function of different wavelengths form a spectrum, which demonstrate the profile of the optical transitions of the target specimen.[2]

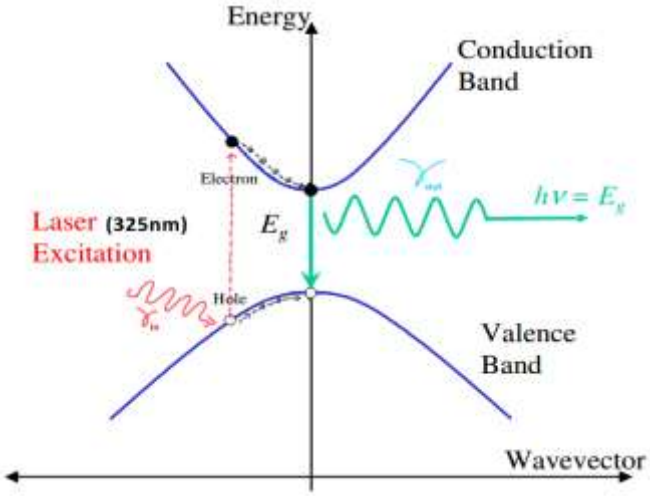

Fig 17, Basic principle of PL

2.2.4 X-ray photoelectron spectroscopy (XPS)

As show in Fig 18, XPS spectra are obtained by irradiating a material with a beam of X-rays while simultaneously measuring the kinetic energy and number of electrons that escape from the top of the material being analyzed. It is a surface-sensitive quantitative spectroscopic technique that measures the elemental composition, empirical formula, chemical state and electronic state of the elements that exist within a material. [3][4]

With X-rays of known wavelength, E_{photon} is known. Then, combine with the measurement of kinetic energy of the emitted electrons, the binding energy of each of these electrons can be determined by the following formula

$$E_{binding} = E_{photon} - (E_{kinetic} + \emptyset)$$

where $\emptyset$ is the work function dependent on both the spectrometer and the material but usually is a constant.

A typical XPS spectrum is a plot of the number of electrons detected versus the binding energy of the electrons detected. Since the binding energies of different electron configurations are in principle unique, they will yield specific XPS peaks correspondingly, allowing us to identify the type of chemical bonds on the specimen surface.

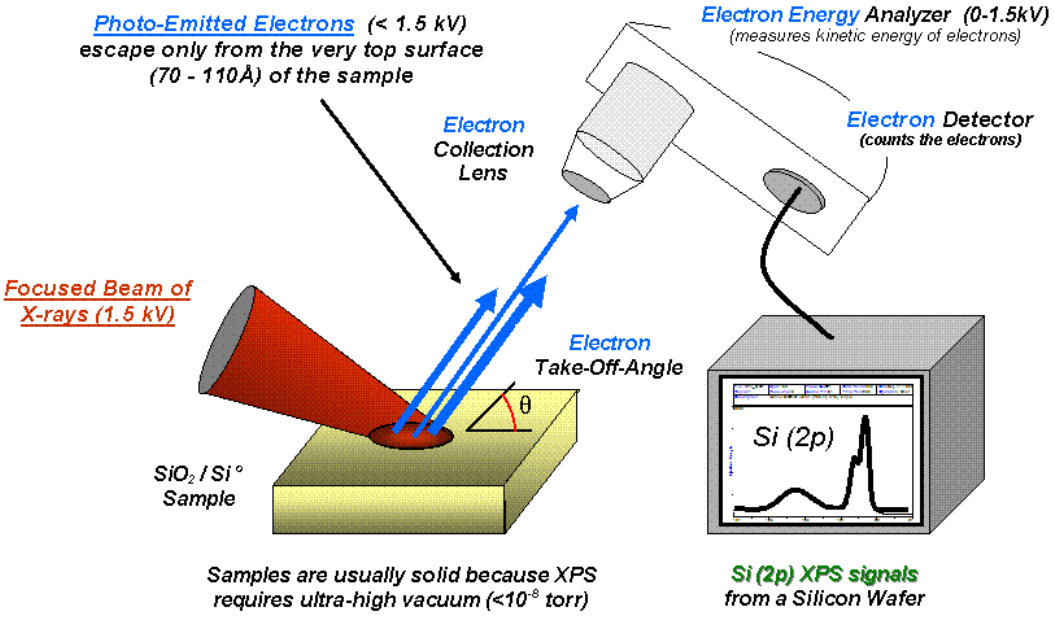

Fig 18, Schematic diagram of the basic components of XPS. [3]

2.2.5 Raman Spectroscopy

Relying on the inelastic scattering of the photon, Raman spectroscopy is a widely-used technique to investigate the vibrational and rotational modes in a material system. A very simple illustration by a Feynman diagram is shown below in Fig 19.

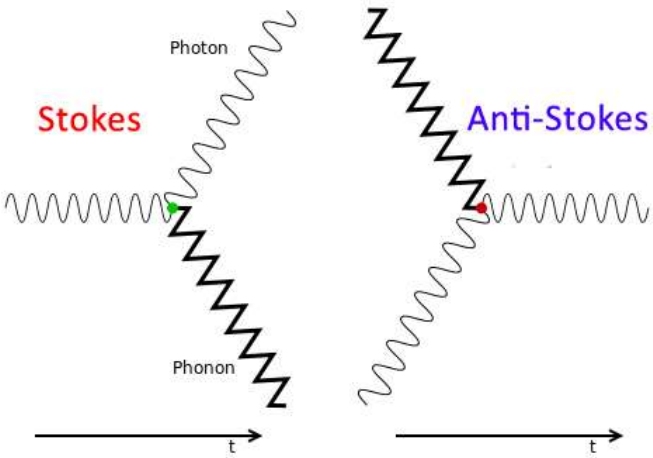

Fig 19, Schematic diagram of Raman Scattering

We can clearly learn from the Feynman diagram that the energy of the incident photon changes after the scattering. This happens because of the interaction of photon with the polarizable electrons and bonds of the molecule. The photon, with a specific wavelength will excite the molecule in either its ground rovibronic state (lowest rotational and vibrational energy level of the ground electronic state) or an excited rovibronic state. The scattered photon can have either lower (Stokes) or higher (anti-Stokes) energy than the incoming photon, depending on whether it create or absorb phonon. The energy difference between the original rovibronic state and this resulting rovibronic state leads to a shift in the frequency of emitted photon from the excitation wavelength. This is the so called Raman shift and we can express it in the following formula:

$$\Delta\omega = \frac{1}{\lambda_0} - \frac{1}{\lambda}$$

$$\Delta\omega(cm^{-1}) = \left(\frac{1}{\lambda_0(nm)} - \frac{1}{\lambda(nm)}\right) \times \frac{(10^7 nm)}{(cm)}$$

Notice $\Delta\omega$ is the Raman shift expressed in wavenumber, λ_0 is the excitation wavelength, and λ is the Raman spectrum wavelength.

Since the vibrational information is specific to the bonds and symmetry of molecules, Raman spectrum is able to provide fingerprint by which the molecule can be identified. [5]

2.2.6 Laser Pruning

One of the key features of this study is the use of focus laser beam to modify the fluorescent ZnO NWs samples.

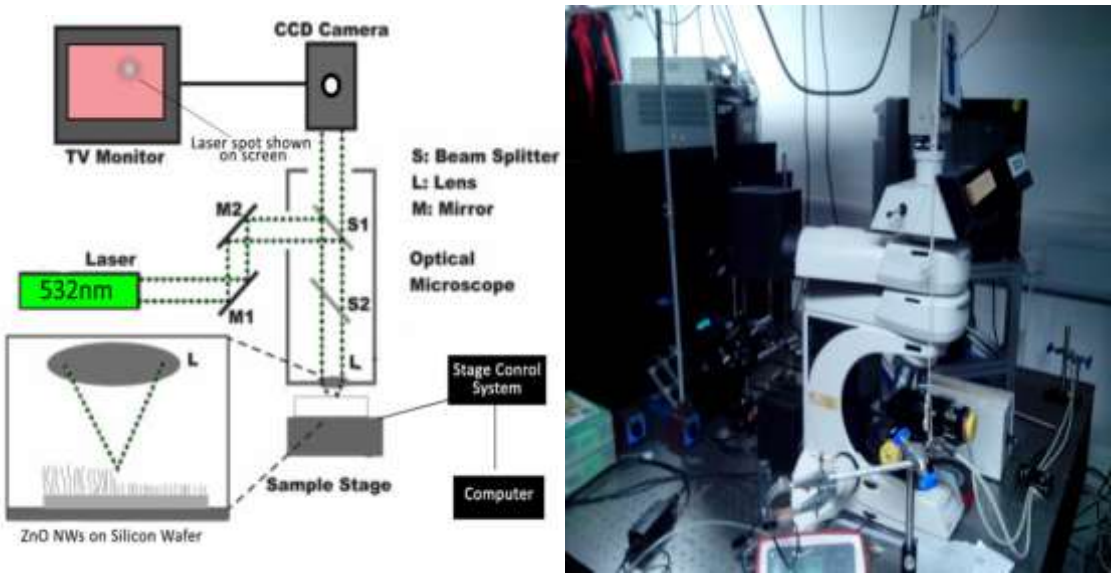

(a) (b)

Fig 20, (a) Schematic diagram of focused laser beam system, (b) Photograph of the focused laser beam setup

As shown in the schematic diagram in Fig 20, a SUWTECH LDC-2500 diode laser (532 nm, maximum power ~ 300 mW) is used to generate laser beam. The emitted beam is then directed into the optical microscope (Leica DMLM) via M1 and M2 reflecting mirrors. After that, the laser is directed to the objective lens (L) via the S1 and S2 dichroic filters. Reaching the objective lens, the laser beam is focused with a magnification of 100x. The spot size of the focused laser beam shooting on the sample surface is ~4μm in diameter. In order to perform precise position control, the sample stage is connected to a computer controlled stage control system (MICOS VT-80 System). With the use of piezoelectric system, a minimum step size of 100nm in X-Y plane is allowed. During the modification process, for viewing purpose the objective lens (L) is also responsible to collect the reflected light from the sample surface. Then, with the use of CCD camera attached on the optical microscope, images of the laser beam on the sample surface can be captured and shown on a TV monitor, allowing us to inspect the laser processing. [6]

2.2.7 Scanning Electron Microscopy (SEM)

Having a de Broglie wavelength of ~10^{-2} nm (assume the electron beam energy is ~10^{3} eV), as well as a far larger DOF (depth of focus), SEM allows better resolution of the image of the sample, as compared to normal optical microscope. This makes it becomes widely used in visualizing a variety of nano-structures.[7]

The electron beam of SEM can be generated via thermionic emission or field emission. In this study the latter method is used (Fig 21 (i)), whereby a high electric field is applied on a very sharp tip. The electrons at the tip (cathode) will then tunnel into the vacuum, propagating in the direction towards the anode.

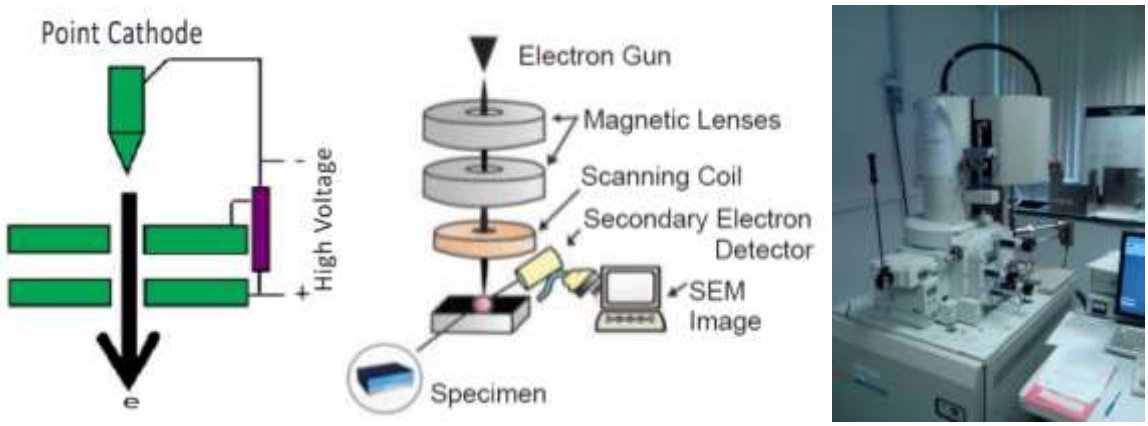

(i) (ii) (iii)

Fig 21, (i) Schematic diagram of field emission, (ii) Schematic diagram of SEM (Adapted from [7]), (iii) Photograph of SEM

As shown in Fig 21(ii), directed by the magnetic field, the electrons will pass through a series of condenser lenses. After that, it will be deflected by the scanning coil to the position of interest.

When the electron beam interacts with the sample, there are a number of signals of distinct types able to be detected. As shown in Fig 22, the incident beam will strike on the specimen surface, colliding with the electrons on it. During the collision, some of the electrons will then be expelled out as secondary electron (SE). The scattered, incident electron beam will usually continue diving deeper in to the sample. During the journey, it keeps colliding with the nearby electrons, causing some of the electrons to be sufficiently energetic to escape from the sample, forming SE2. On the other hand, the incident electrons also have an opportunity to "U-turn" after a series of collisions, and come out from the specimen. We call this kind of electron backscattered electron (BSE). However, it is possible that the BSEs continues traveling until being reflected by the objective lens, forming secondary electron 3 (SE3).

In our study of ZnO NWs, secondary electron imaging (SEI) was used to observe the pattern of the nanowires on the sample surface.

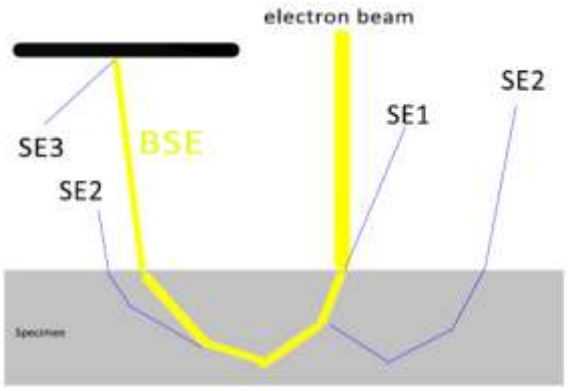

Fig 22, Schematic diagram of different SEM signals. The central, thickest beam represents the incident electron beam. [8]

2.2.8 Energy-dispersive X-ray spectroscopy (EDX)

With reference to Fig 23(a), in performing EDX, external stimulation such as high-energy protons or a beam of X-rays is used to excite the inner-shell electrons of the atom. Gaining enough energy, the electron will escape from the atom. This leaves a "hole" at the shell, allowing electron from outer shell to de-excite and take over the "hole". The de-excitation from higher energy level to lower energy level will lead to the release of X-ray (the emission wavelength is in the order of 10^{-12}m~10^{-8}m) corresponding to the energy difference.

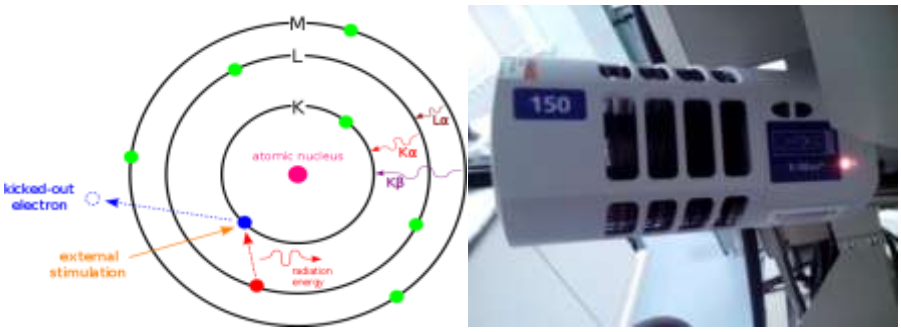

(a) (b)

Fig 23, (a) Schematic diagram of EDX [16], (b) EDX module attached on the SEM system.

The number density and intensity of those emitted X-rays are captured by the spectrometer. By plotting intensity versus energy of X-ray, EDX spectrum with a series of peaks can be obtained.

Since every element has its unique energy difference between the shells, EDX technique is capable of identifying the elemental composition of the target specimen.

2.2.9 Transmission Electron Microscopy (TEM)

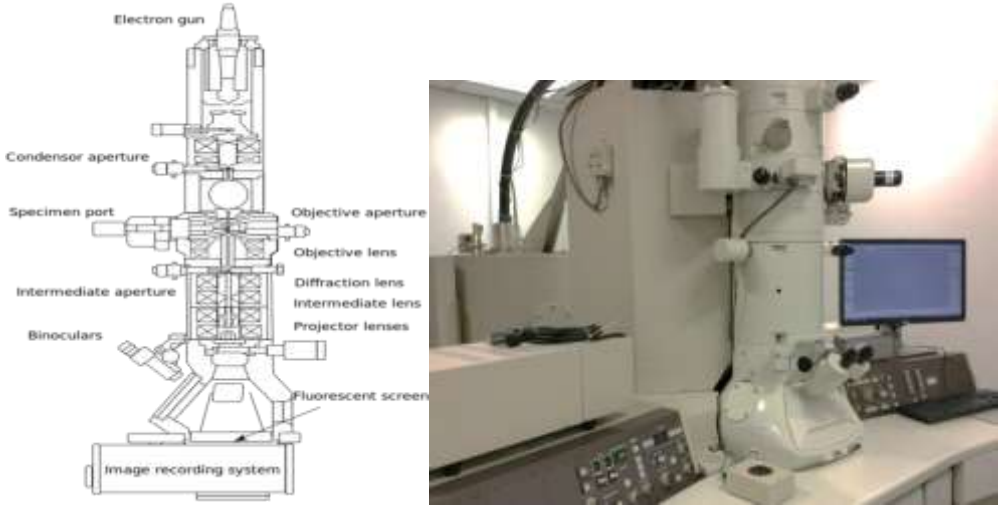

(i) (ii)

Fig 23, (i) Schematic diagram of TEM, (ii) Photograph of TEM in EM lab of NUS chemistry department.

As shown in Fig 23, although the schematic diagram looks more complicated than in the case of SEM, the working principle of TEM before the electron beam strikes on the specimen is similar. The difference lies in the way of imaging.

In TEM, as suggested by the term T for transmission, the incident electrons will transmit through the specimen. Then these outgoing electrons will land on the fluorescent screen under the specimen, generating light at points where they hit. In this way, the brighter region of the image formed on the fluorescent screen will represent area of specimen where more electrons were transmitted, while darker region will represent area where less electrons were transmitted, which is also where the atoms located. The image on the fluorescent screen is then passed down to the image recording system where magnification and other adjustments are conducted. [9]

The resulted image will typically have a good resolution up to the atomic scale, allowing us to measure physical quantities including the lattice spacing.

References

[1] Spring KR, Davidson MW. "Introduction to Fluorescence Microscopy". Nikon MicroscopyU. Retrieved 2008-09-28 (Adapted from http://www.microscopyu.com/articles/fluorescence/fluorescenceintro.html)

[2] “Compendium of Chemical Terminology, 2nd ed”. (the "Gold Book") (1997)

[3] B.V.Crist, “Handbooks of Monochromatic XPS Spectra”, Volumes 1 and 2, published by XPS International LLC, 2005, Mountain View, CA, USA.

[4] J. F. Watts, J. Wolstenholme, “An Introduction to Surface Analysis by XPS and AES”, published by Wiley & Sons, 2003.

[5] Gardiner, D.J., “Practical Raman spectroscopy, Springer Science and Business Media”, (1989).

[6] Yan Ru Choi, Minrui Zheng, Fan Bai, Junjun Liu, Eng Soon Tok, Zhifeng Huang, Chorng Haur Sow, “Laser-induced Greenish-Blue Photoluminescence of Mesoporous Silicon Nanowires”, SCIENTIFIC REPORTS | 4 : 4940 | DOI: 10.1038/srep04940.

[7] Chin Wee Shong, Sow Chorng Haur, Andrew TS Wee, “Science at Nanoscale: An Introductory Textbook”, Pan Stanford Publishing Pte. Ltd., 2010.

[8] Supplementary Video- Ho Yi Wei, Hew Kai Ming, ”SP2251 2014 Scanning Electron Microscope”, 2014. Adapted from: https://www.youtube.com/watch?v=xbFFpCboR9E

[9] Williams, David B., and C. Barry Carter. "Transmission Electron Microscopy Plenum." New York, NY (1996).

Chapter 3

Results and discussions

As mentioned before, this project contains two parts： i) find out the scheme(s) to produce sample with emission profile of interest, ii) investigate the effect of laser beam on the sample surface.

3.1 Control of the resulted emission of as-prepared sample

The emission profile of the sample can be mainly tuned during the growth stage. Like the case of semiconductor processing, the outcome will rely on the flux diffusion and the surface reaction rate. In fact, all the manipulations work to provide different degrees of flux diffusion and surface reaction rate. We found that the emission profile is very sensitive to the contribution of the two factors.

3.1.1 Mass ratio of precursor components

One of the ways to tune the fluorescence of the ZnO NWs sample is the manipulation of the mass ratio of the precursor.

Ideally, to achieve maximum yield of Zn at the source region, we require same mole of both Zn and C. Translating into mass ratio, we need to mix 6 portions of Zn with 1 portion of C. However, in reality we are unable to demand all reactants to interact and react fully and totally. Thus, using a mass ratio of 6: 1 does not guarantee an optimum growth of the nanowires. In fact, we need more C in order to increase the chance of reducing ZnO but the increasing amount of C also has the possibility of inhibiting the interaction of Zn with the incoming carrier gas. The extent of this effect depends on the way of grinding the mixture and therefore is quite impossible to measure or make any quantification.

Yield optimization is obviously difficult to achieve but mass ratio manipulation is still good enough to give us a rough estimation on the resulted Zn concentration reaching the substrate, while keeping other parameters constant. This way of controlling the Zn concentration or the Zn diffusion flux is more effective than controlling other parameters because it directly changes the amount of Zn by adjusting the proportion of ZnO in the precursor. A proof to its effectiveness is the emergence of emissions other than brown and green, when we increase the proportion ZnO in the precursor. As shown in Fig 25, as the mass ratio of ZnO to C is adjusted to 3: 1, violet fluorescence starts to emerge.

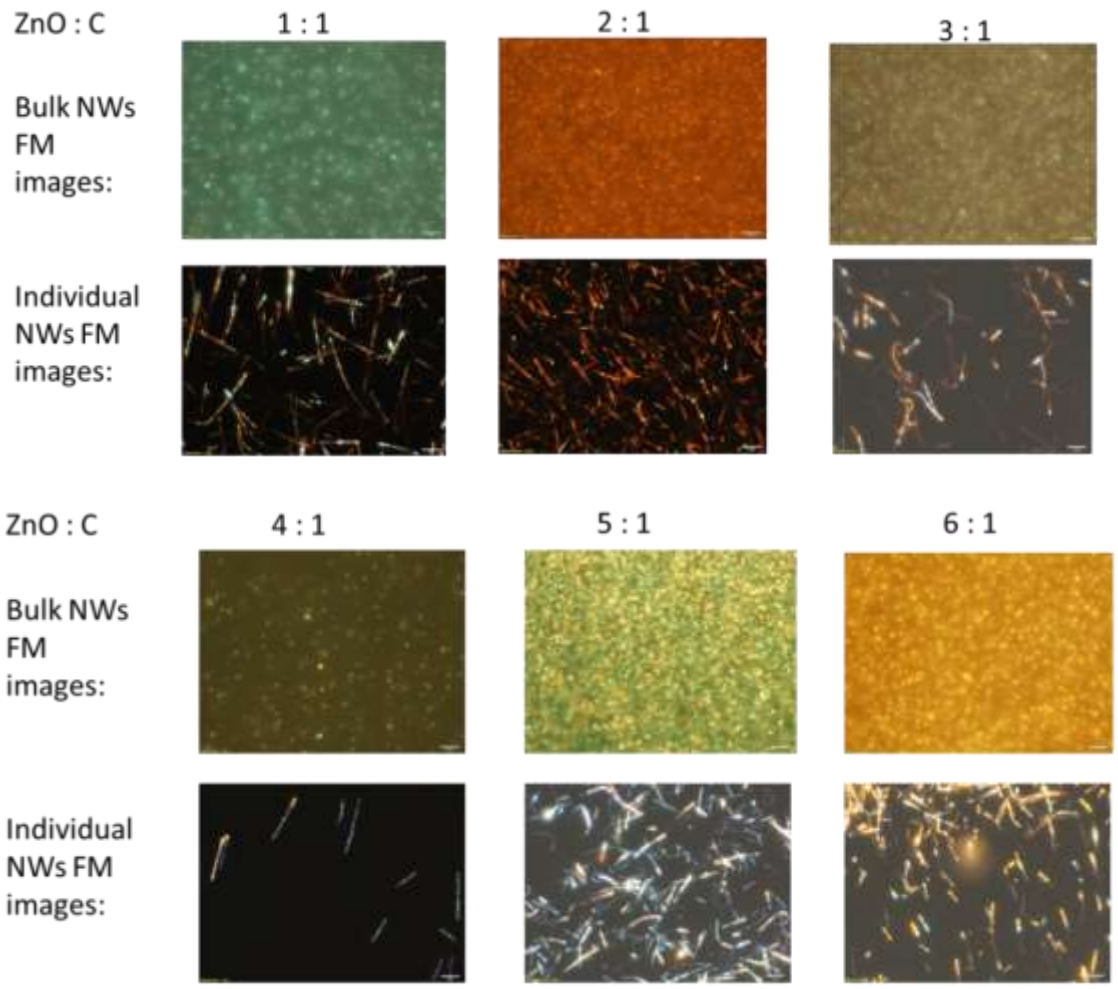

Fig 25, FM images of bulk NWs surface (first row), extracted individual NW (second row). The above six samples were grown under similar conditions (15cm from precursor, synthesized at 850°C) except with different ZnO: C mass ratios. The scale bars in all images are 5 μm.

As shown in Fig 26, the relative intensity of PL peak near the violet region increases with the proportion of ZnO in the precursor.

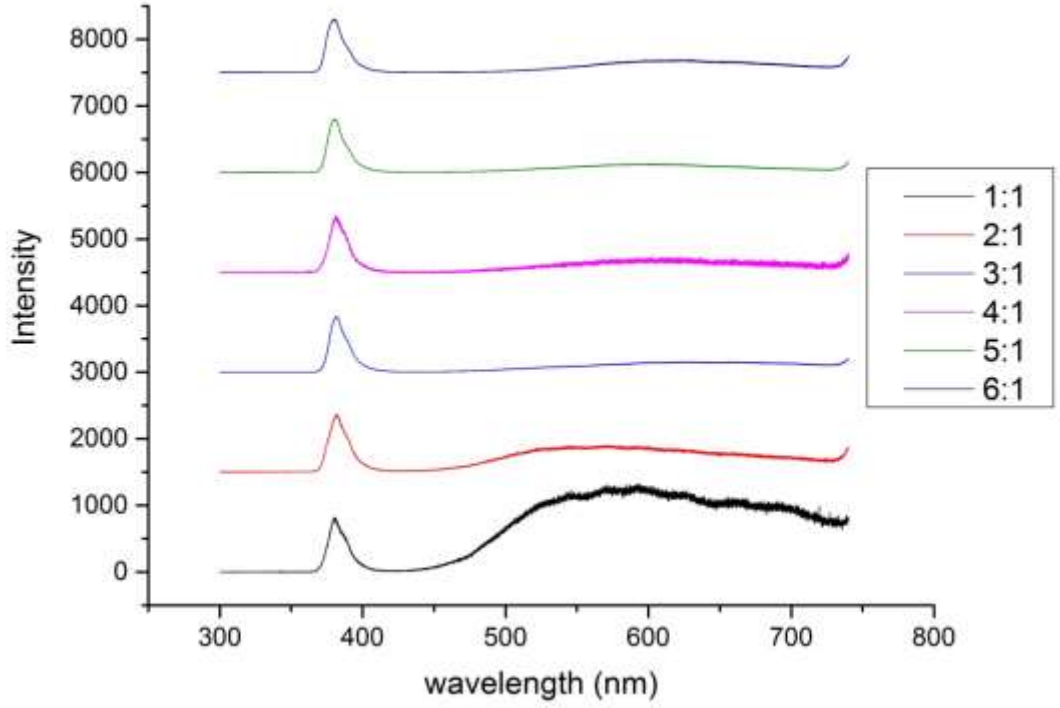

Fig 26, Combine PL spectra of samples with different ZnO : C mass ratios.

For more details, we tried to quantify the color profile by measuring the length of different color segments of a number of nanowires (see Fig 27) and then from there we roughly estimate the average proportion of different emissions (see Fig 28).

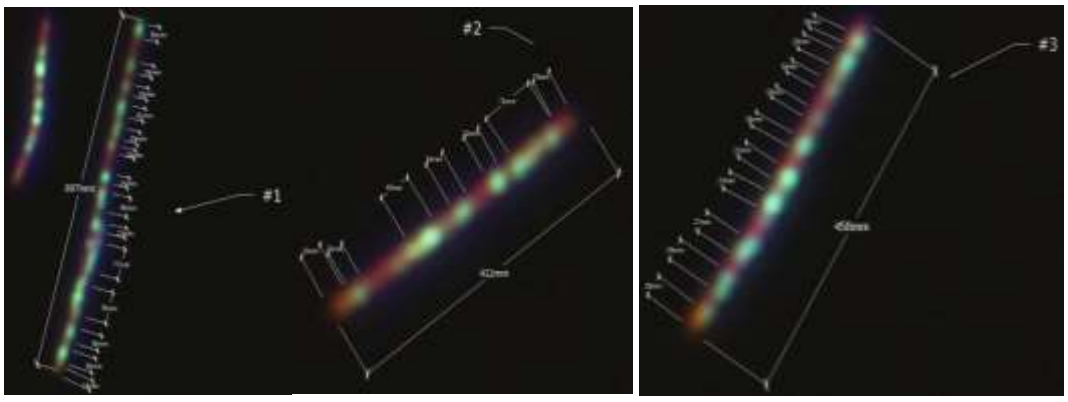

(i) (ii) (iii)

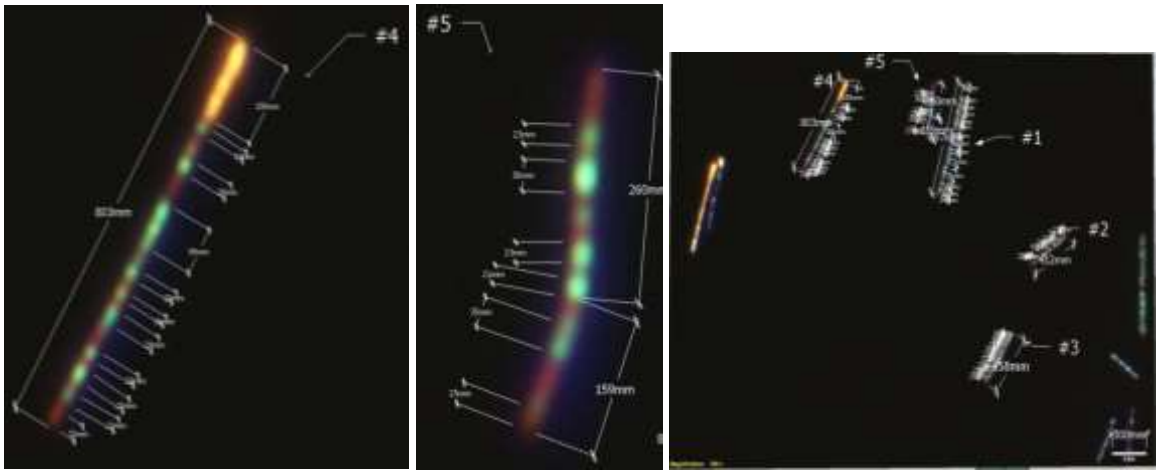

(iV) (V) (Vi)

Fig 27, A typical image processed by Google Sketch-up. Notice the lengths measured here do not imply the real length. In fact, it is not to scale and in this case the scale is 5 µm to 300 mm or 1 µm to 60 mm. Image (i) to (V) are the magnified images while (Vi) is the original FM image.

Mass ratio	Purple	Brown	Green
4	47.1	10.3	42.6
5	18.4	21.2	60.4
6	39.3	40.2	20.5

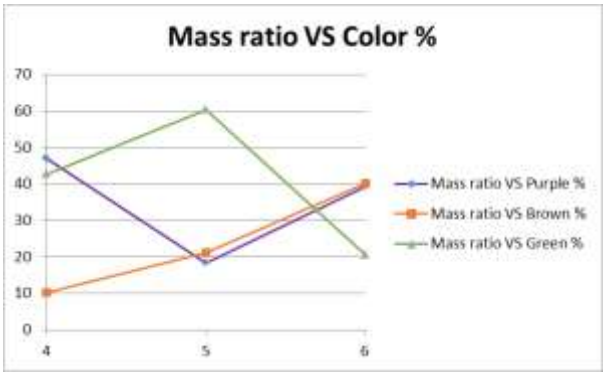

Fig 28, A rough estimation of the proportion of different colors from nanowires at one spot.

We can observe from the result shown in Fig 28, that percentage of brown emission increases with the ZnO proportion in the precursor. This indirectly agrees with our suggestion on the relationship between Zn concentration and brown emission. On the other hand, percentage of either green or violet does not have a well-defined trend.

A possible explanation with reference to Haibo Zeng's model (refer to Fig 8) is that the probability of transition between Zn_i-levels and Deep levels is more dominant than between Zn_i-levels and Valence

band (VB), as well as between Conduction band (CB) and Deep levels. In simple language, violet and green emission must compete with the brown emission in addition to their own transition probabilities. The exact explanation may need a more rigorous theoretical formulation using DFT.

3.1.2 Position of substrate

As mention earlier, there are actually two types of position parameter, i.e. the position of the substrate and the position of the quartz tube within the furnace.

The position of substrate affects the diffusion flux of the source material (which is Zn in our case) onto the substrate surface, and this will determine how well the growth of nanostructures. On the other hand, changing position also alters the temperature of the substrate due to the non-uniform temperature distribution inside the CVD furnace.

As shown in Fig 29, we can notice that beyond 10cm from the center of the furnace, the temperature change over a short distance becomes very drastic. This temperature alteration in turn changes the surface chemical reaction rate at the substrate surface, implying the change in the interaction with the incoming oxygen, and thus affecting the nanowires growth too. Another problem is that the error bar becomes larger at distances further away from the center of the furnace. This means that the temperature at the same position may not be very consistent. Therefore, this also raises the issue of inability to reproduce exactly the same collection of parameters for each synthesis run.

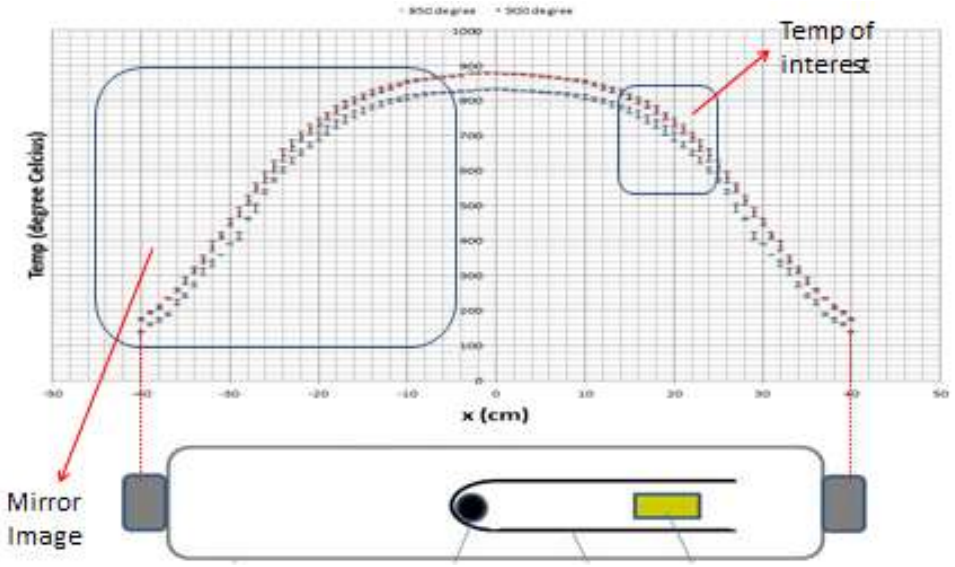

Fig 29, Temperature profile inside the CVD furnace. The red curve refers to the profile when the set temperature is 900°C while the blue curve refers to the profile when the set temperature is 850°C. The x-axis represent the distance from the center of furnace.

Two synthesis schemes:

a) Scheme A: Using a long substrate to produce different fluorescence along it

In this growth scheme, substrate with length of 4~5cm were utilized. The emission or fluorescence along the sample is not uniform, as shown in Fig 30. This is also applies to the density of growth of the nano-structures, according to their respective PL intensities and SEM images.

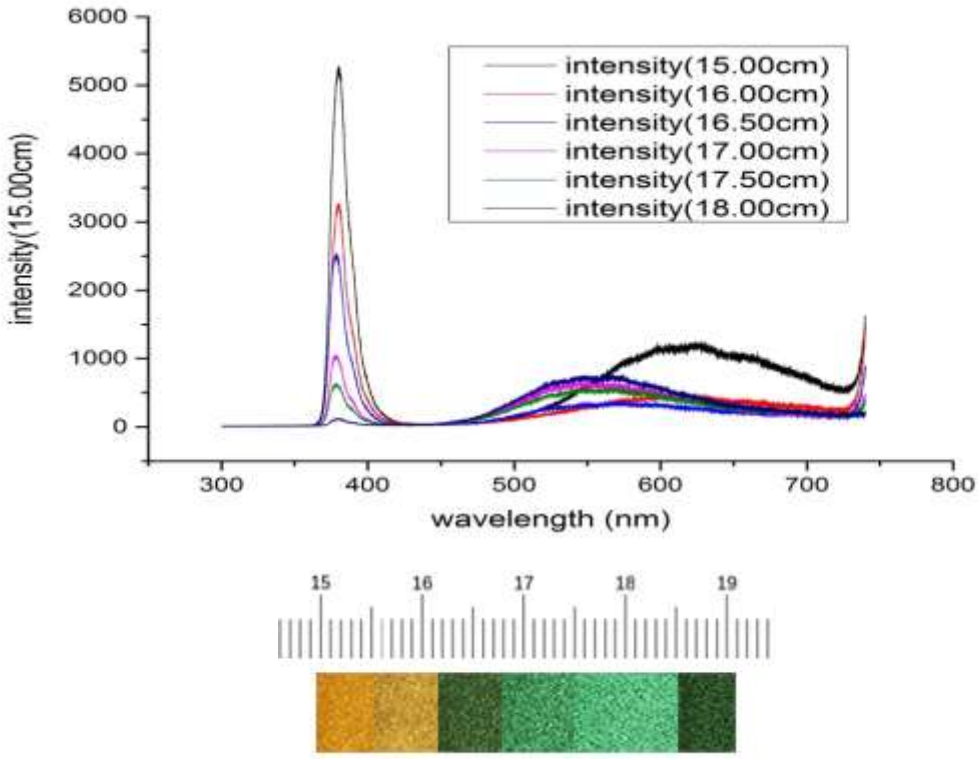

Fig 30, A typical PL profile of a long sample. Notice as the distance from the source increases, the overall intensity of the PL spectrum decreases. Below is the FM color spectrum along the sample. Notice the colors of fluorescence are quite different at different position.

The main problem of this growth scheme is that nano-structures grow badly at the far end (wrt source) of the substrate.

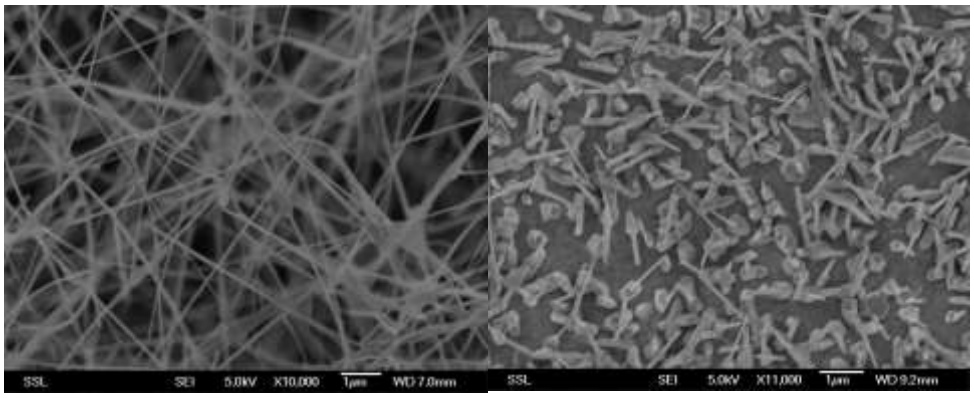

(a) (b)

Fig 31, SEM images of a typical long sample. Image (a) is taken near the upstream edge (~15.00cm), while image (b) is taken near the downstream edge (~19.50cm).

As shown in Fig 31, the resulted profiles are quite different between the two positions. In particular, the density of nanowires at (b) is obviously far less than that of (a). Intuitively, this result was initially deemed to be due to the depletion of source materials upon reaching positions further away. However, similar situation happens when we tried to grow with a shorter substrate while maintaining the amount of precursor. This seems to suggest that the amount of precursor may not contribute too much on this kind of outcome.

In the light of Chun Li's work on the growth of GeS [2], we then begin to consider the effect of gas flow boundary layer. The schematic diagram of this model is shown in Fig 32.

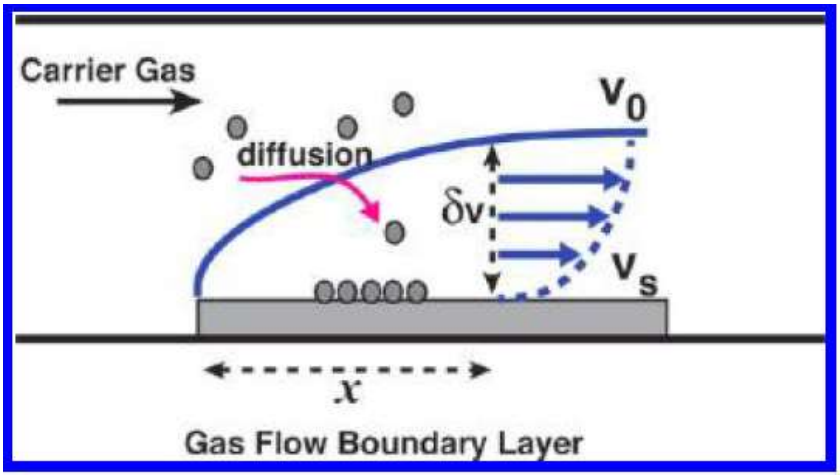

Fig 32, Schematic illustration of the diffusion of source materials through the gas flow boundary layer. The velocity gradient boundary layer is indicated by a solid blue curve. V_0 and V_s are the gas velocity in the bulk gas flow and at the surface of the substrate. δ_v is the thickness of the boundary layer. x is the lateral distance away from the upstream edge of the substrate. The horizontal arrows indicate a gradual change of gas velocity in the

boundary layer. (Adapted from Chun Li, Liang Huang, Gayatri Pongur Snigdha, Yifei Yu and Linyou Cao, "Role of Boundary Layer Diffusion in Vapor Deposition Growth of Chalcogenide Nanosheets: The Case of GeS", ACS Nano, 2012, 6 (10), pp 8868–887)

In short, it proposes that as the lateral distance away from the near end (upstream edge) of the substrate increases, the thickness of the gas flow boundary layer becomes thicker.

$$\delta(x) = \sqrt{\frac{\mu_g}{\rho_g B}\frac{P_{tot}}{T' J_c}x}$$

The above equation suggests how the thickness $\delta(x)$ relates to the distance x from the near end. (The terms μ_g, P_{tot}, ρ_g, B, $T'$and J_c represent the dynamic viscosity of the gas flow, total pressure, density of gas flow, gas constant per cross-section area, local temperature of the substrate and the molar flow rate of the carrier gas.)

By assuming a linear concentration gradient across the gas flow boundary layer, we can express the diffusion flux as

$$\frac{dm}{dt} = -D\frac{P_{par} - P_s}{\delta(x)} = -D\sqrt{\frac{\rho_g B T'}{\mu_g}}[P_{par} - P_s(T')]\sqrt{\frac{J_c}{P_{tot}x}}$$

where D is some kind of diffusion rate constant, P_{par} is the partial pressure of the source materials and P_s is the equilibrium vapor pressure of source materials at temperature T'. The above expression shows that the diffusion flux is proportional to $\frac{1}{\sqrt{x}}$ and $\sqrt{T'}$. For $\frac{1}{\sqrt{x}}$, directly we can see it is decreasing with distance from the near end, while for $\sqrt{T'}$, strictly speaking it does not depend on x, but rather depend on how far the position from the hottest zone (furnace center) of the furnace. However, as far as this study is concerned, the far end of the substrate is always pointing away from the hottest zone, T' is always decreasing with distance too. Therefore, the value of both two factors decrease with x, leading to the decrease of diffusion flux at the far end.[2]

This shows that the problem lies within the gas flow along the substrate rather than the amount of the precursor. As evidence, in one case two substrates were placed at different positions (5cm and 22cm) inside the quartz tube.

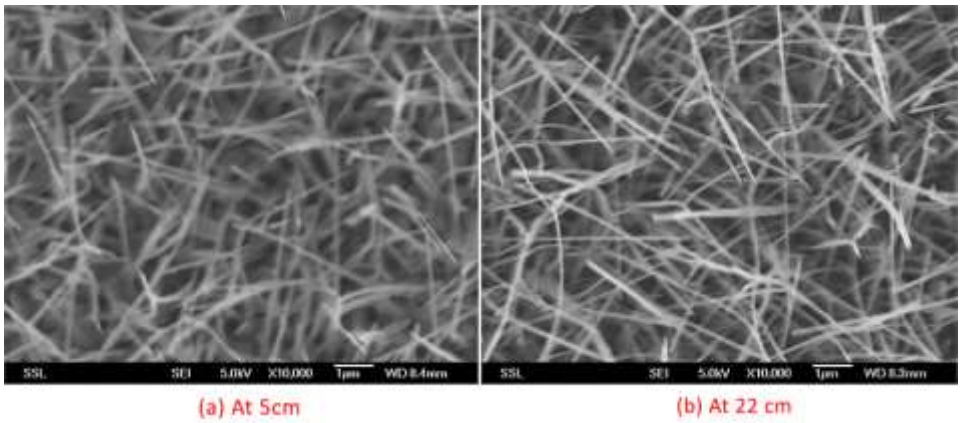

Fig 33, a) SEM image taken on sample synthesized at 5 cm from the precursor, b) SEM image taken on sample synthesized at 22 cm from the precursor.

The growth of nanostructures on both samples is quite good, as shown in Fig 33. This indicates the use of segmented substrates if we want to study how the nanostructures change along a large distance.

b) Scheme B: Using a square substrate

Another growth scheme is the use 1cm x 1cm samples. The purpose of this growing manner is to investigate the emission profile at a certain position with minimum disturbance from neighboring regions. For instance, we can then study the effects of diffusion flux and temperature on the resulted emission or fluorescence.

However, the problem is both the flux and temperature are position-dependent, and both decrease in their values with distance. This raises the difficulty to study how dominant the two factors in contributing to the result as compared to each other.

To solve this problem, we assume there is no change in temperature within ±10 cm from the center of the furnace. This means shifting the position of the source within this range does not change its temperature. However, with reference to our temperature profile shown in Fig, this does not applies to the substrate region because the a change of more than 20°C can be induced by a slight shift of 2cm. By making use of this fact, as well as the assumption that the flow rate of gas is more dominant than temperature in determining the diffusion flux, we are then able to have different temperature at the substrate region while roughly maintaining the diffusion flux at that position.

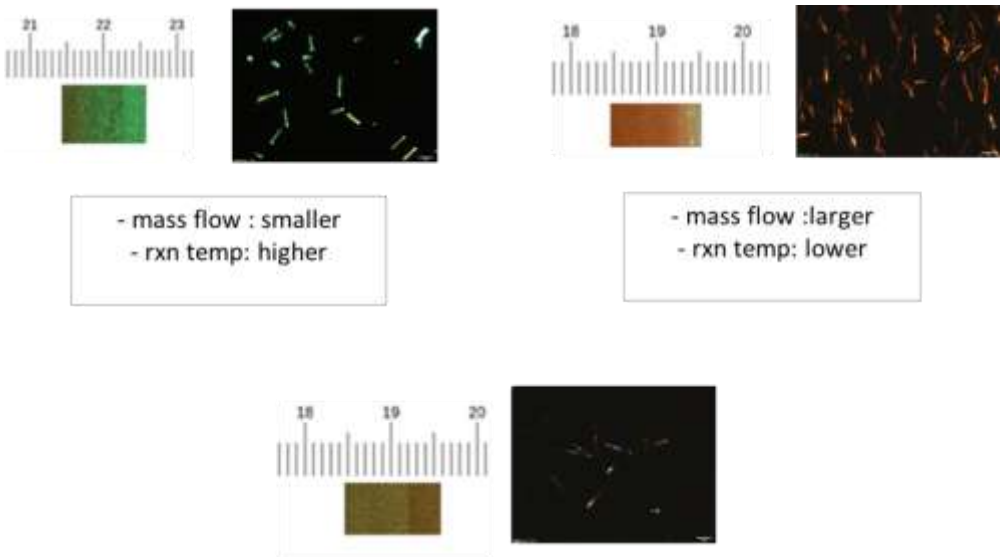

Fig 34, Fluorescence of both bulk NWs surface and extracted nanowires grown under different diffusion and temperature conditions. The bottom shows the null case.

To investigate how the above mentioned two factors actually affect the dominant fluorescence, we synthesized three samples under similar conditions except a slight change (~2cm) on the position of either the substrate or the quartz tube. The fluorescence of the three samples are shown in Fig 34.

Let the bottom sample be the null case. In order to have a higher temperature (while keeping the mass flow wrt null case) at the substrate, the quartz tube was shifted 2cm inward. The resulted fluorescence under UV excitation is shown at the top left of Fig. The sample appears more greenish. On the other hand, to obtain a greater mass flow, the substrate itself was shifted inward while the quartz tube remained unchanged. This time the sample appears more reddish, as shown at the top right of Fig 34.

Notice the change in bulk surface also applies at the scale of individual nanowire. Thus, we can conclude without researching in depth the exact underlying principles, that the shift between diffusion flux limit and surface reaction limit is crucial in altering the dominant fluorescence of the as-prepared sample. Possible reasons may again rely on the density of state (DOS) of the Zn_i-levels, which is believed to be proportional to the Zn diffusion flux, and also the DOS of deep levels which is deemed to be due to the reactions with oxygen and thus is temperature-dependent.

3.1.3 Oxygen Concentration and Post-Synthesis Oxygen Annealing

The amount (concentration) of oxygen is also affecting the out-coming emission. In addition to working during the synthesis process, oxygen treatment can also be conducted after the sample has been grown.

From the synthesis chemical equation (2), we know that either the Zn or the O_2 behave as the limiting factor, depending on their relative molar concentration with respect to each other. When oxygen concentration is lower, excessive Zn particles may not be able to find their partners and this will lead to the formation of oxygen vacancies. Similarly, if the situation is reversed then Zn vacancies may also appear. For other defects like interstitial and anti-site, the formations are rather by chance, but very likely the higher the concentration of the element, the higher the probability of forming those defects of that element.

The control of oxygen concentration can be done by connecting the gas inlet to gas tank with the required oxygen concentration. The laboratory only possesses tanks of mainly two concentrations, 0.5% and 1%, and in our case this concentration difference is not large enough to indicate the contribution of oxygen concentration to the resulted emission. To address this, we purposely create a certain degree of leakage to allow the introduction of some amount of atmospheric air during the synthesis.

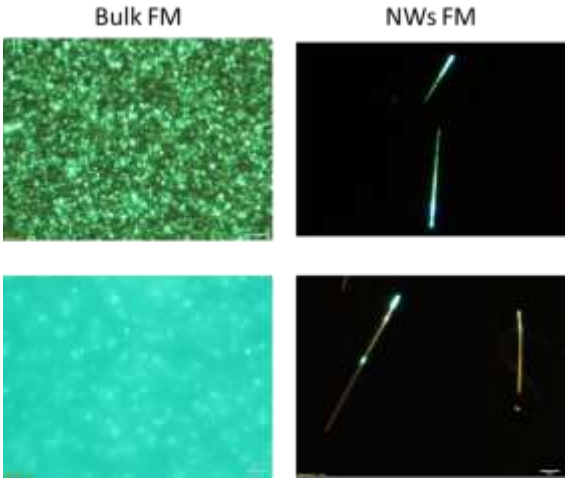

Fig 35, FM images of two kinds of green sample. The upper sample was subjected to higher oxygen concentration during the synthesis because of leakage. The bottom sample was grown without leakage at an oxygen concentration of 1%. Notice although both of them emit green fluorescence, their individual nanowire behaves quite differently.

As shown in Fig 35, both two higher or lower oxygen concentrations are able to produce green fluorescence. However, their individual nanowires are quite different. Under higher oxygen

concentration, the nanowires appear green too; under lower oxygen concentration, the nanowires are mainly brown even its bulk surface appears green.

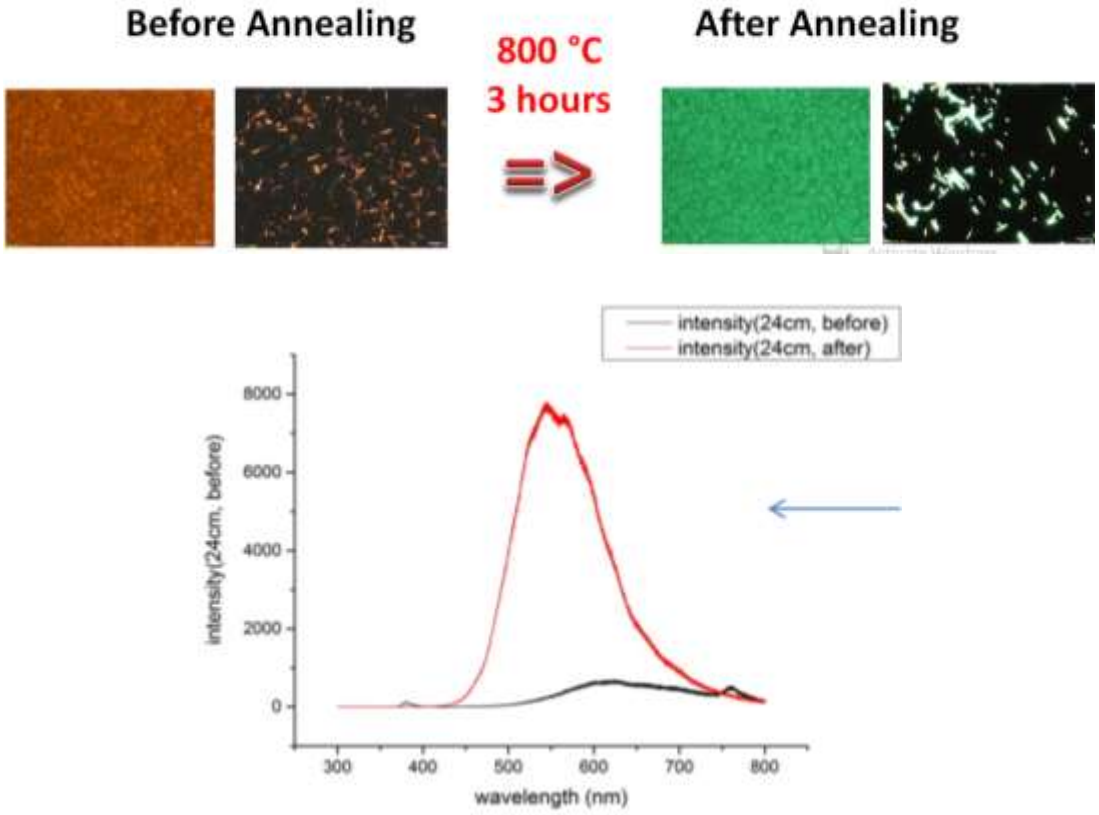

Fig 36, FM images of both bulk NWs surface and individual nanowire before and after oxygen annealing in atmosphere. Below are their respective PL spectra.

As mentioned in the beginning, oxygen treatment is also doable even after the synthesis process. By annealing the brown sample in an open air ambient at 800°C for 3 hours, both the bulk NWs surface and individual nanowire become green, as shown in the upper part of Fig 36. PL spectra at the bottom of Fig 36 show great increment in the intensity at the visible range. This outcome is indicative of the increase of defects after annealing.

Both the above cases suggest the role of oxidation in providing additional defect levels (in this case, deep levels), and thus changing the fluorescence of the ZnO NWs.

Although the full picture is not clear yet, we still can deduce that oxidation plays a significant role in altering the fluorescence of ZnO NWs sample. However, the alteration by annealing has its backdrop of not being localized. In order to achieve precise, localized modification on the as-prepared sample, we require a kind of tool which induces changes at reasonably small spot size.

3.2 TEM and XPS study on Green- and Brown-fluorescence specimen

TEM:

Recalls in the section 3.1.3, ZnO NWs are suspected to exhibit core-shell-like structure. To verify, single green and brown NW are investigated respectively using TEM technique. The results are displayed in Fig 37. Images (a) and (b) show that the lattice spacing of a single green-fluorescence NW is measured to be 0.28 nm. The value is similar to the ZnO lattice spacing in the [1010] direction, indicating the NW is constituted by ZnO molecules. On the other hand, images (c) and (d) show that the single brown-fluorescence NW seems to be encapsulated by a "shell" with a thickness in the range of 2 nm to 4 nm. While the core's lattice spacing is consistent with the result obtained from the green-fluorescence NW, the shell's lattice spacing of 0.265 nm does not belong to any of ZnO-related lattice spacing. The closest ZnO's lattice spacing is 0.260 nm, the lattice spacing in the [0002] direction. Yet the discrepancy is still too large in the case of lattice spacing measurement, so we cannot claim that the "shell" comprises ZnO molecules too. A possible explanation is the incorporation of carbon atom, either in the form of interstitials or even in the form of ZnC by replacing the oxygen atom. With the belief that the ZnC is very unstable, it is likely to have a larger ionic radius, thus causing larger lattice spacing. To further prove this argument, XPS technique may be useful in investigating the existence of carbon-related bonding. [3]

XPS:

As suggested in the previous section, XPS measurement is conducted in order to investigate the existence and nature of carbon within the ZnO NWs. The results are displayed in Fig 38. In all following cases, the raw XPS spectra are fitted with appropriate peaks using the XPS Peak Fit software.

The top left image of Fig 38 compares the typical Zn2p peak of green-fluorescence (Sample A) and brown-fluorescence (Sample B) ZnO NWs sample. Sample A and B have peaks centered at 1021.4 eV and 1021 eV respectively. This is an indirect evidence showing sample A has more zinc-oxygen bonding. Conversely, it also hints the replacement of atom other than oxygen atom which results in a weaker bonding and thus smaller binding energy. In this case, the primary suspect is carbon atom. [3]

On the top right of Fig 38, the relative intensity of O2- peak (530.1 eV) to VO (oxygen vacancy) peak (531.8 eV) in both sample A and B can be clearly observed. Obviously, sample A has a lower value in such relative intensity, indicating sample A possesses more VO defects than sample B. This result shows that the contribution of VO is likely to be insignificant to the brown fluorescence. On the other hand, the higher relative intensity in sample B might also suggest the filling of carbon atoms into those vacancies. [3]

Finally, at the bottom of Fig 38, carbon-related peaks are studied. In particular, we managed to obtain typical graphite peak (284.6 eV) and another carbon-related peak corresponding to C-O bonds, in both sample A and B. However, sample B has an additional peak found at 282 eV. This peak is then attributed to Zn-C bonds by elimination rule. The reason of not considering Si-C bonds is due to its large formation energy corresponding to temperature range between 1430 and 1510 °C .[4] Its lower value in binding energy agrees with the argument made with reference to the result of Zn2p peak. [3]

In short, with reference to TEM and XPS results, we argue that the incorporation of carbon atoms or the bonding of carbon to Zn atom contribute to the brown fluorescence of the NWs. Besides, the weak binding energies of carbon-related peaks also suggest the possibility of the replacement of carbon back to oxygen under certain circumstances. This behavior is useful when we discuss on the possible mechanisms of laser modifications.

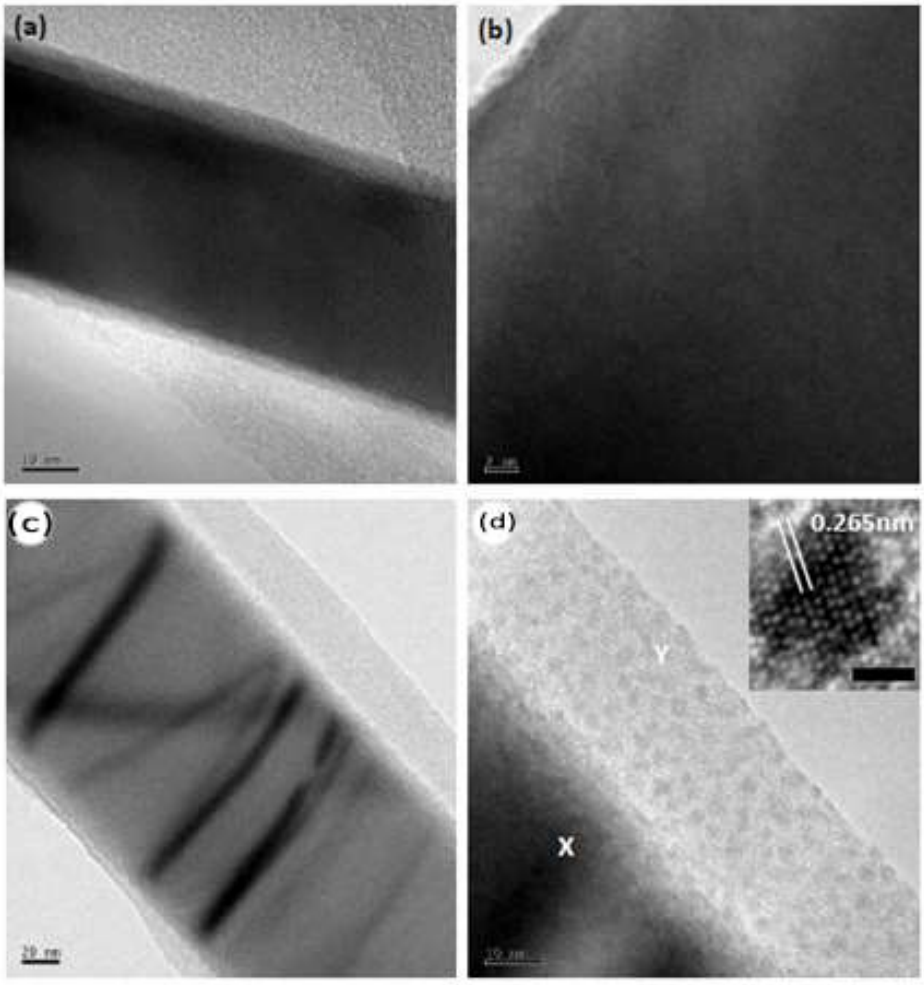

Fig 37, (a) and (b) are taken from a single ZnO NW of green fluorescence while (c) and (d) are from ZnO NW of brown fluorescence. [3]

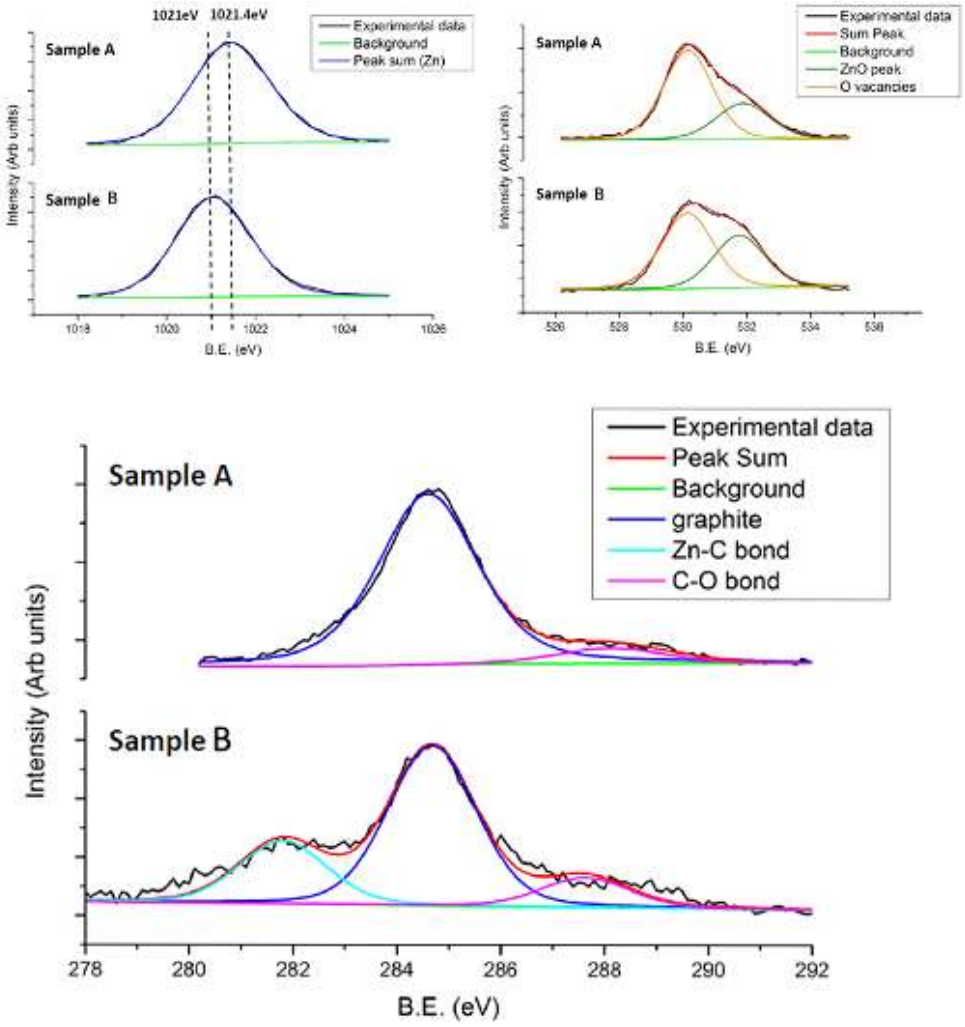

Fig 38, XPS spectra of green-fluorescence ZnO NWs (Sample A) and brown-fluorescence ZnO NWs (Sample B). [3]

3.3 Laser Modification

The as-synthesized sample is irradiated with a focused laser beam directly at room temperature and pressure. Two incidents are considered to be highly probable to happen: thermal disintegration of the surface structure of the as-grown sample and induced chemical reactions at the sample surface. Both incidents depend mainly on thermal excitation due to the absorbed photon energy from the focused laser beam.

3.3.1 Disintegration by laser beam in brown and green samples

Due to low absorption coefficient [5], green-fluorescence ZnO NWs usually appear transparent to laser in the range ~532nm. In other word, it is quite unlikely that the sample will absorb the energy of photon and react accordingly.

In our case, since the fluorescence of the sample can be tuned to brown, it is believed that the ZnO NWs might then have a different absorption coefficient which allows it to react upon being bombarded.

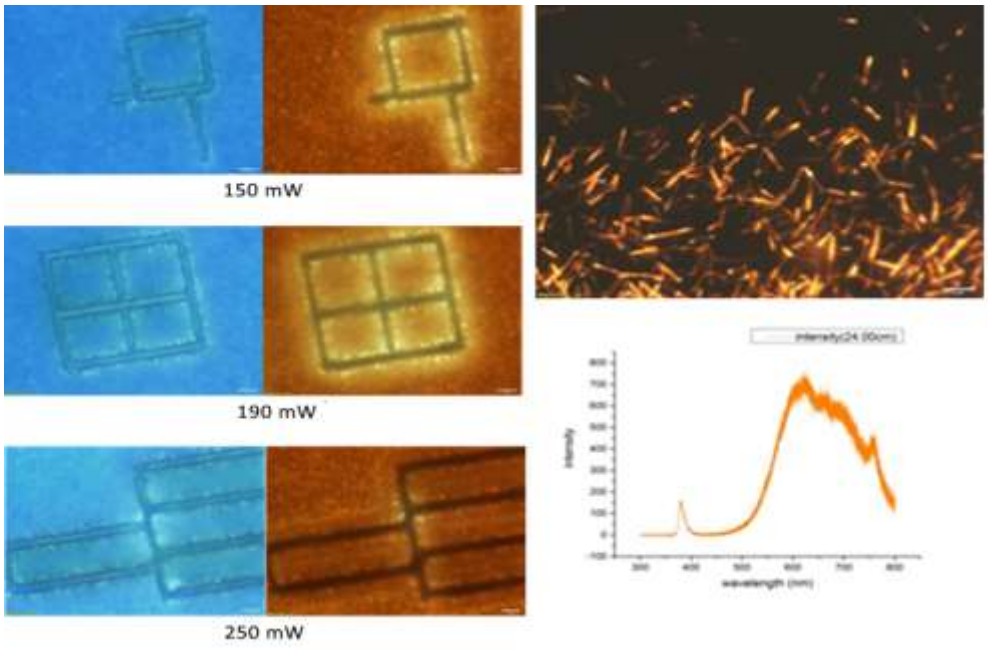

Fig 39, Laser modification on a brown ZnO NWs sample. Optical images and FM images were taken. The two images at the bottom are the FM of extracted nanowires and the PL spectrum.

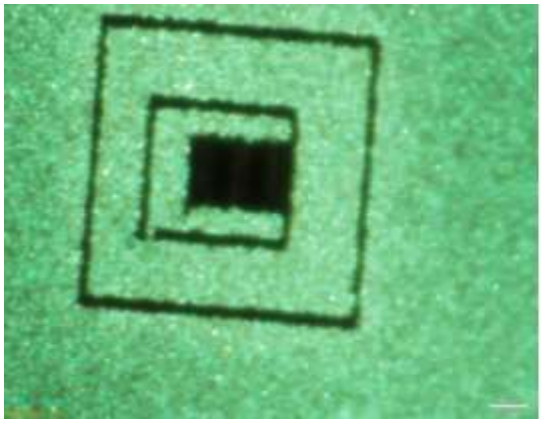

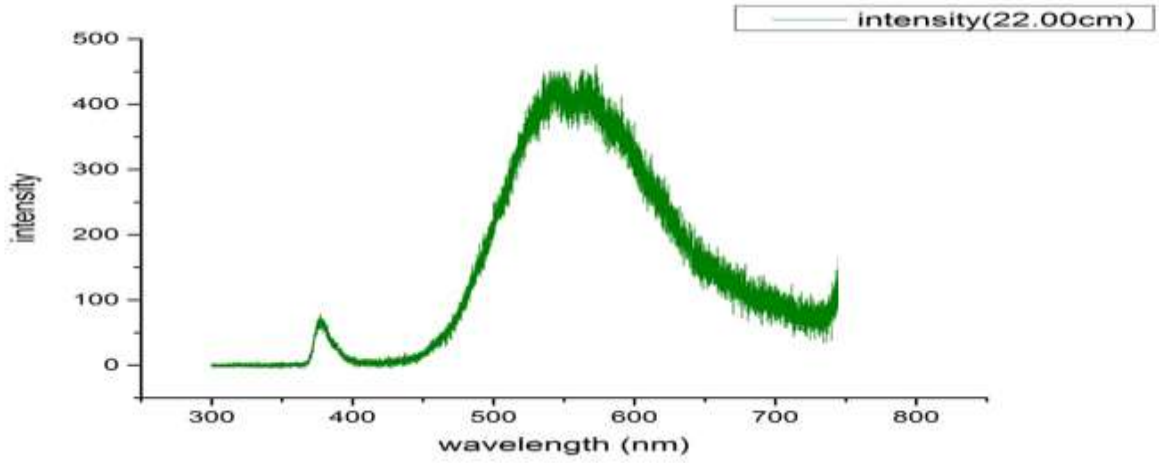

Fig 40, Laser modification on a green ZnO NWs sample. FM of bulk and individual nanowire are shown. Notice the extracted nanowires are mainly brown even though the bulk surface appears green. Below is the corresponding PL spectrum.

As shown in Fig 39 and Fig 40, we found that disintegration can happen in both brown and green samples. Notice the green sample here is not the commonly-seen green ZnO NWs sample and in reality from its extracted nanowires, it is clearly seen that its dominant fluorescence is still brown.

A possible cause of the above observations is the existence of vast amount of Zn-C bondings in brown-fluorescence nanowires, as discussed in the previous section. These weak bonds, being induced by laser beam, easily react with oxygen in the atmosphere, forming CO or CO_2. The exothermic reactions may also produce thermal energy which causes local disintegration of the bombarded region by melting the nano-structures.

3.3.2 Brown-green fluorescence alteration by laser beam

Recall the brown sample in Fig 37, the regions near the cut edges seem to have slight change in their fluorescence. Also inspired by Lu's work, this leads us to consider the possibility of photo-chemical reaction induced by focused laser beam.[6]

In fact, this mechanism works well on ZnO NWs too. As shown in Fig 40 and 41, we can make use of laser beam to achieve precise and localized fluorescence modification and create some interesting patterns or write some secret messages, which can only be visualized under UV excitation.

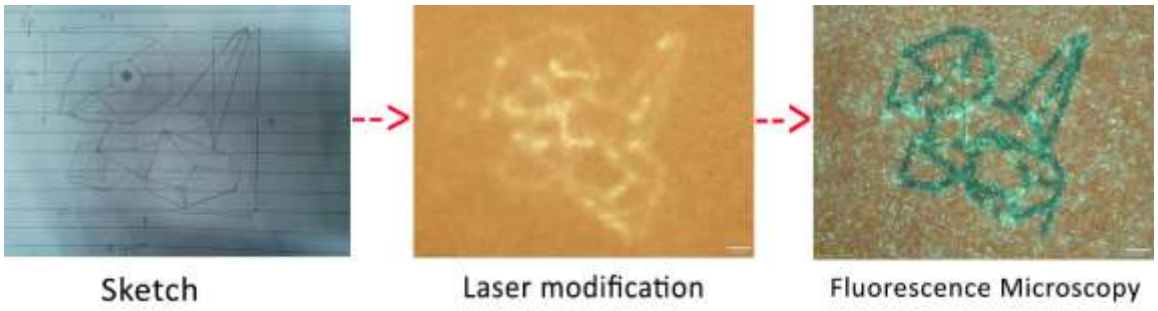

Fig 41, Steps to draw Porygon on the surface of the ZnO NWs sample.

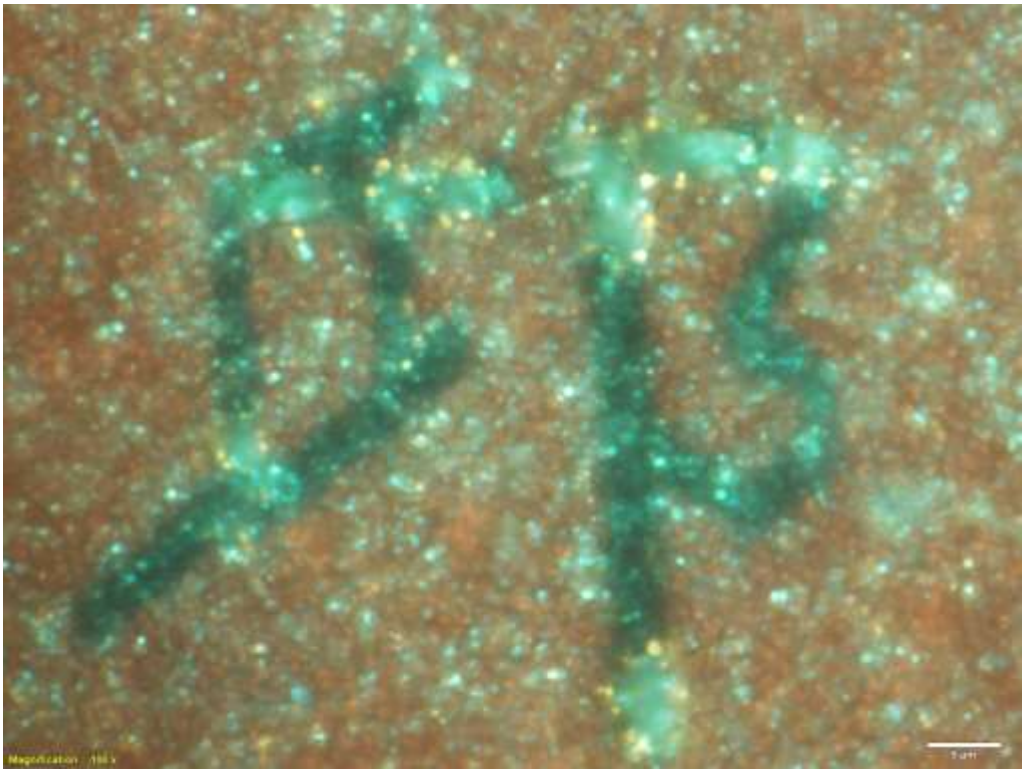

Fig 42, The ability of fluorescence alteration by laser beam allows us to write secret messages on our sample at micro-scale.

In another occasion, we managed to alter the color of a brown-fluorescence sample into green, as shown in Fig 43. PL results also show the quench of emission beyond 600 nm after laser modification.

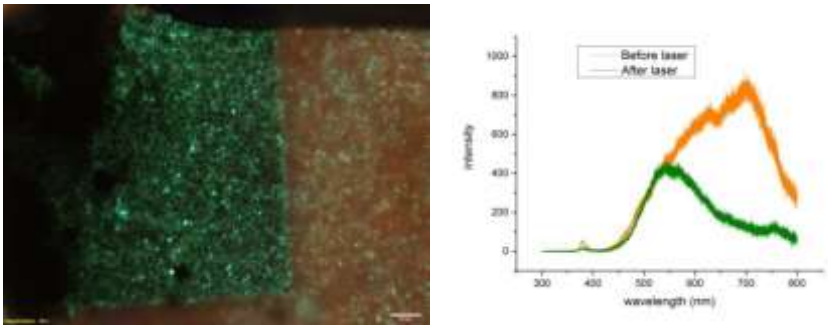

Fig 43, LHS: FM image of the laser-modified sample. The modification was done at the top right corner with an area of 100x100 μm^2. RHS: PL spectra taken at region with and without laser modification

The next thing we decided to figure out is the minimum critical power to induce the color change. The purpose is to find out an optimum range of power which does not change the morphology of the nanowires drastically. For instance, we do not hope to see the melting of nanowires as displayed in the bottom image of Fig 45. Different laser powers haven been used, as shown in Fig 44. It was found that with a power higher than ~25 mW, the outcome becomes consistent, while for power lower than ~25 mW, almost nothing happens. From here, we can deduce that the minimum power to induce the color change is approximately 25 mW.

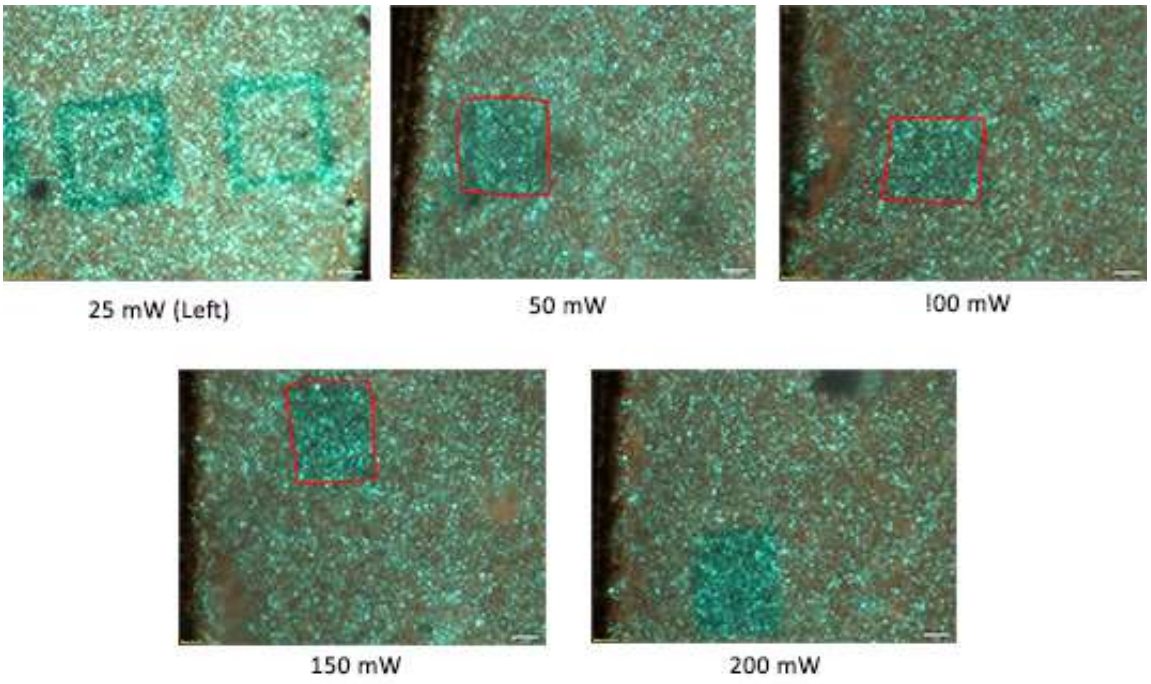

Fig 44, FM images of an as-prepared sample after laser modification with different powers. Greenish squares of area 20 µm x 20 µm were drawn using focus laser beam.

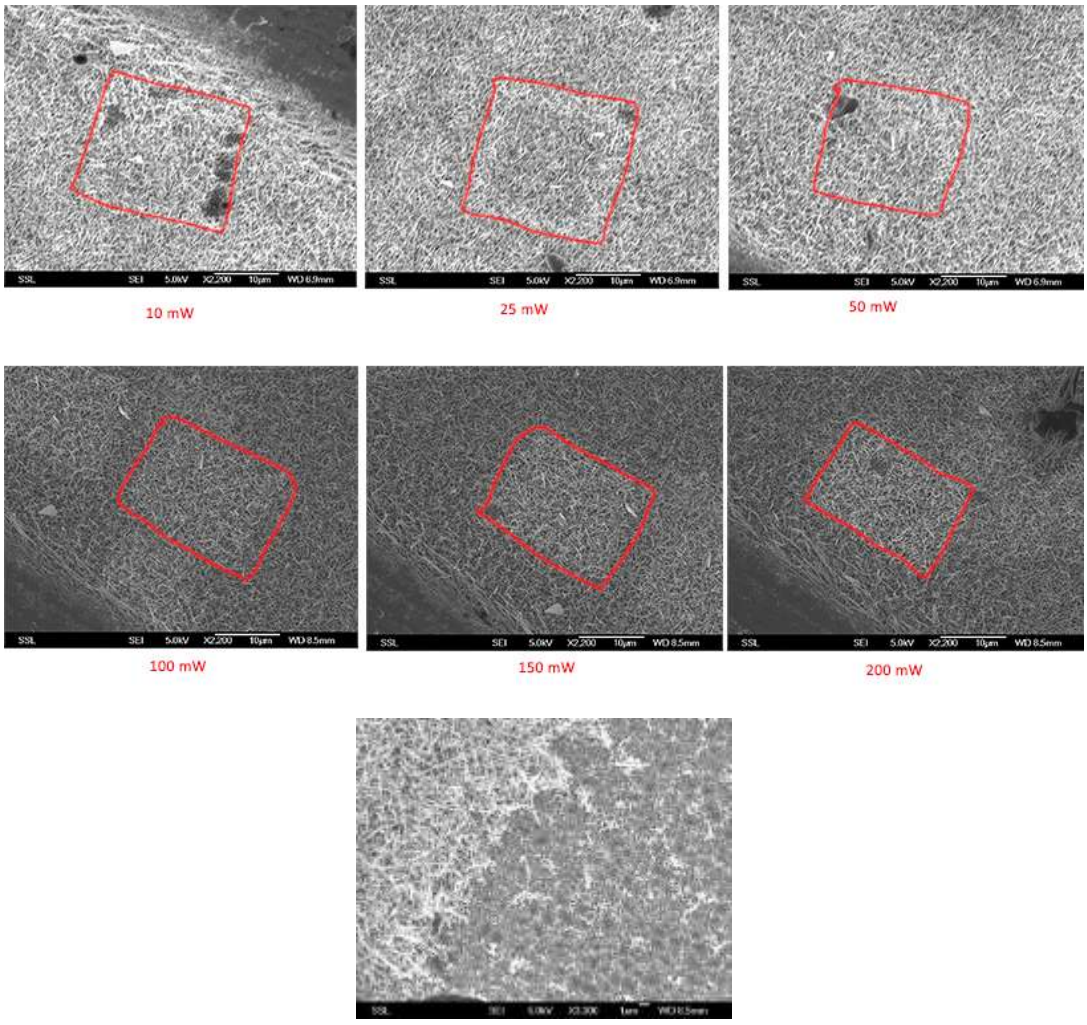

Fig 45, SEM images of regions modified by laser beam with different powers. Notice when the laser power becomes too high, the nanostructures were melted.

In order to further characterize the those regions, PL and Raman spectroscopy were also conducted as shown in Fig 46 and Fig 47. From PL spectra in Fig 42, we can see the quenching of intensity at region beyond 600 nm as the laser power increases. This seems to suggest the laser beam has eliminated some of the defect levels originally existing on the specimen.

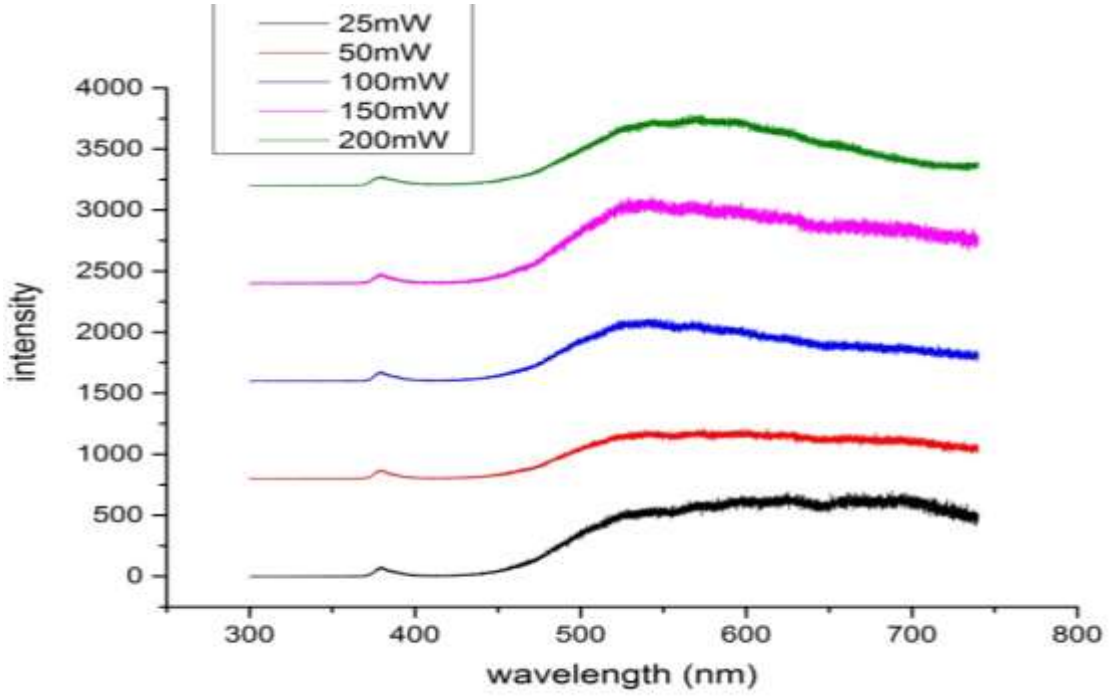

Fig 46, PL spectra collected at regions modified with different laser powers

Raman spectra in Fig 47 then provide us a possible explanation to what happens during the irradiation of focused laser beam. As shown in Fig 43, besides the well-known peaks related to ZnO A1 and E2 mode, there are also peaks at 1336 cm^{-1} and 1582 cm^{-1}. Initially, we assume the impurity contributes insignificantly to the profile of the specimen, so the two peaks were attributed to some ZnO multi-phonon interactions (A1(LO)+A1(TO)+E2 and A1(LO)+A1(TO)+E1+E2 respectively).[7] However, Shrama et al.'s work has suggested that these modes, locating at 1360 and 1460 cm^{-1}, were barely visible after post-synthesis UHV (ultra-high vacuum) annealing. Thus, these peaks should not be so clearly visible if we normalize the spectrum to the Si peak. This leads us to consider the modes which are not originated from ZnO but some other element, and in this case, carbon. This argument is deem valid since it is likely some of the carbon (graphite) moves along with the Zn flux and lands on the substrate during the synthesis under specific conditions and are incorporated into the sample. The peaks with the closest wavenumbers as compared to our results (1336 and 1586cm^{-1}) are found to be the diamond's triply degenerate mode (1332cm^{-1}) [8] and graphite E2g mode (1575cm^{-1}) [9]. This looks better except it does not explain the reason which causes the broadness of the two peaks in our results. Another seemingly more persuasive explanation might be the D- (1300-1400cm^{-1}) and G-band (1500-1600cm^{-1}) of graphite.[10] In this case, the two peaks are attributed to the breathing mode sp2 atoms and the bond stretching of pairs of sp2 atoms respectively.[11] Combined with the fact that sp3 states are negligible for visible excitation while sp2 states always resonate with visible excitation [12], the assignment of D- and G-band seems to be more convincing. In any case, this suggests the existence of carbon structures on the specimen. Both carbon-related peaks experience decrease in intensity as the

power of the focused laser beam increases. What possibly happens is the oxidation of these embedded carbon structures into carbon monoxide or carbon dioxide. By conservation law, the release of these products will reduce the amount of carbon on the specimen surface. In correspondence to the color change, this in turn suggests that the carbon structures are very likely in contributing to the yellow-related deep levels as described in the energy band diagram. A possible example from first principle calculation provided in Tan's Work is the (C_{Zn}+2O_i) acceptor level.[13] Thus, with the decrease of these deep levels, the transitions related to yellow emissions will decrease too, resulting in a more green-dominant emission or fluorescence profile.

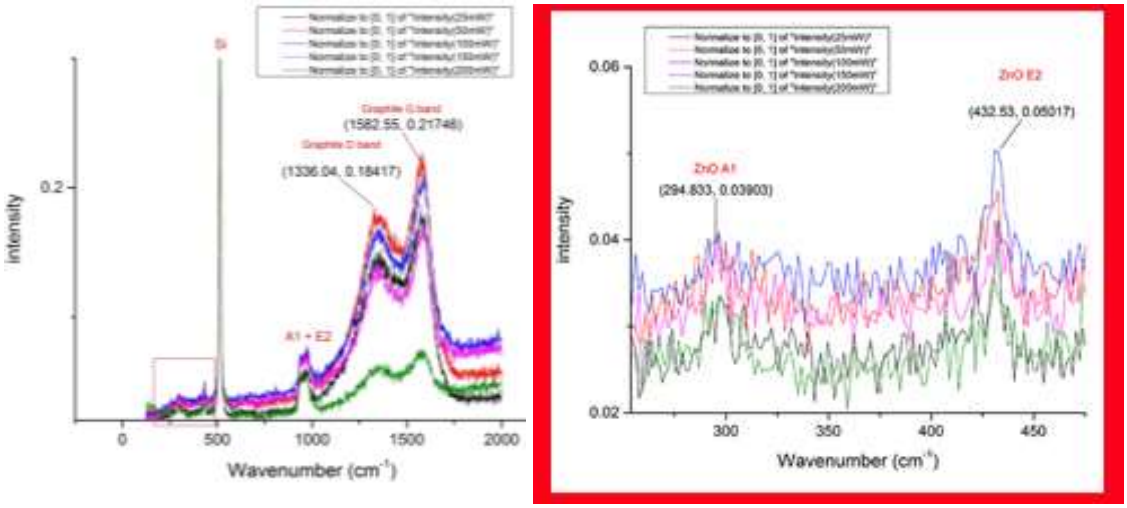

Fig 47, LHS: Raman spectra collected at regions modified with different laser powers. The peaks are due to different modes of ZnO or Graphite, RHS: The enlarged results enclosed in the red rectangle in LHS.

To further verify this argument, we made use of the EDX technique to estimate the quantity of elements including Zn, O and C at regions modified by laser beam with different power.

Before the discussing the quantitative results, a rough mapping of different elements onto the SEM image of interest is shown in Fig 48. The mapping results of Zn and O from (b) and (c) respectively show clearly that the densities of Zn and O are higher on the region with nanowires but lower at region without nanowires. In the case of carbon, due to its smaller atomic percentage (shown in Fig 49 and 50), its overall density over the entire region is therefore lower, resulting in a poorer mapping pattern, especially at the left part (d). However, the right part of (d) is still presenting us the pattern of nanowires as seen in both (a) and (b). Besides, the region where the empty pentagon seen in (a) and (b) locates, obviously contains less red dots and thus has a relatively low density as compared to regions with nanowires. Thus, we are still able to claim that the result in (d) is similar to (b) and (d). As a result, we can conclude that the three elements, Zn, O and C are mainly residing on the NWs.

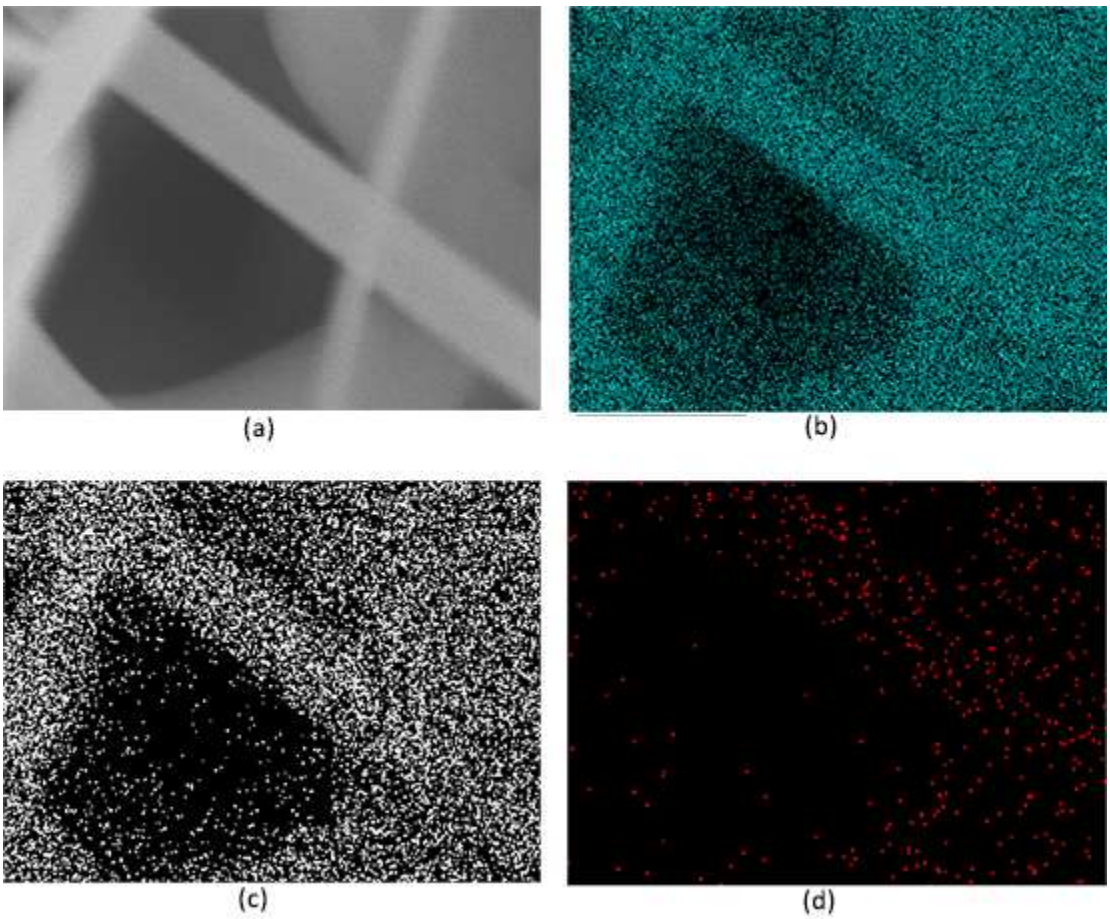

Fig 48, EDX mapping of elements. (a) SEM image of the region of interest, (b) Mapping of Zn using blue dots, (c) Mapping of O using white dots, (d) Mapping of C using red dots.

Next, the atomic percentage of different elements is studied via the EDX spectrum. As shown in Figure 49 (a) to (e), EDX spectra corresponding to different laser powers were displayed. The elements are quantified by calculating the area under the peak of each identified element and after taking account for the accelerating voltage of the beam to produce the spectrum. For our convenience in, we further convert the values into atomic percentages.

Fig 49(a), EDX spectrum and elemental composition at region modified by laser with 0mW power.

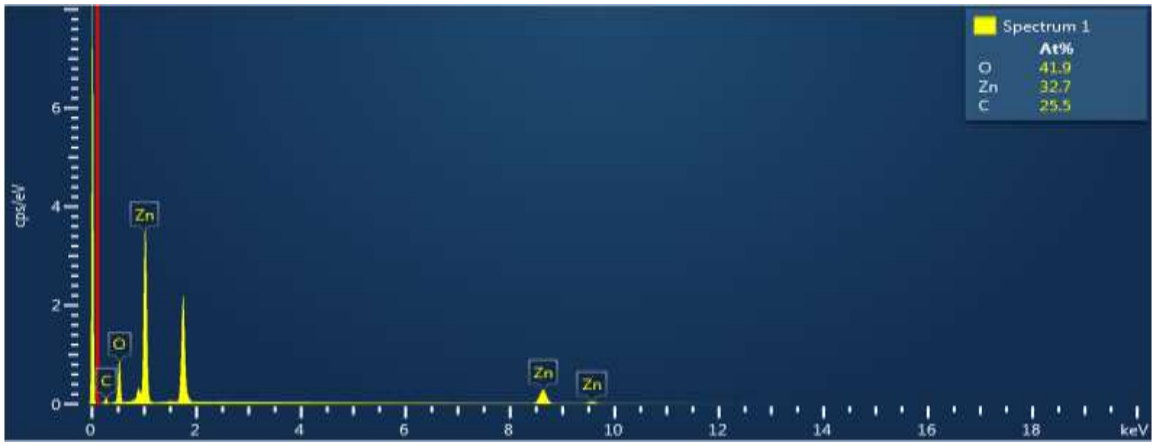

Fig 49(b), EDX spectrum and elemental composition at region modified by laser with 25mW power.

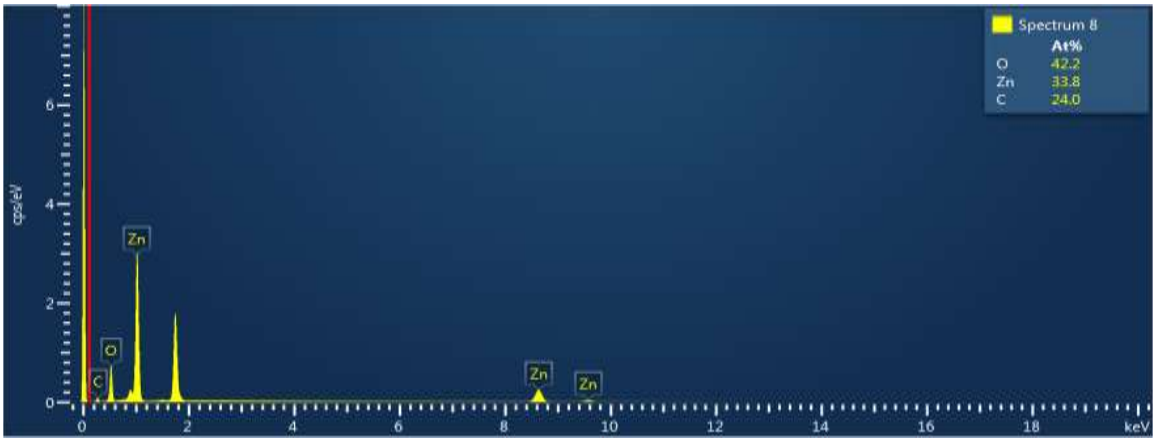

Fig 49(c), EDX spectrum and elemental composition at region modified by laser with 100mW power.

Fig 49(d), EDX spectrum and elemental composition at region modified by laser with 25mW power.

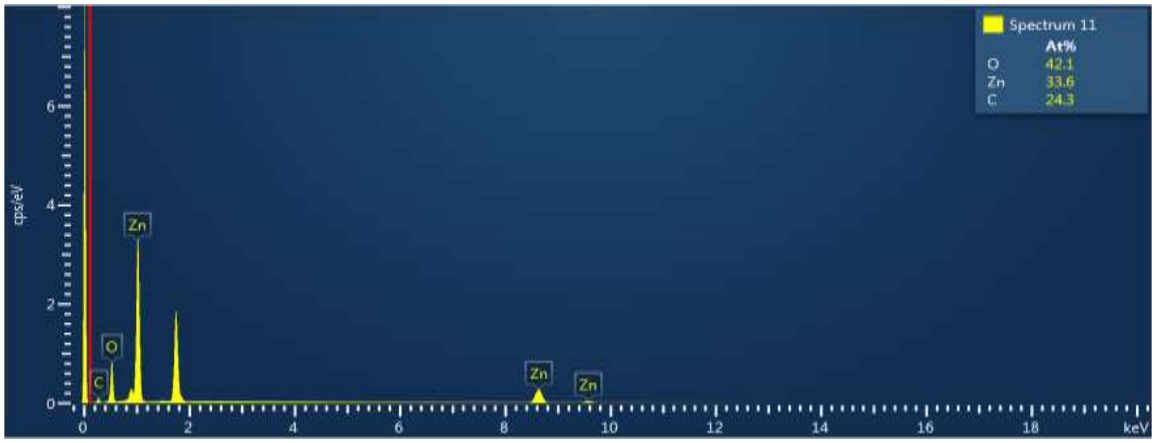

Fig 49(e), EDX spectrum and elemental composition at region modified by laser with 25mW power.

In order to have a clearer visualization on how those quantities of elements change with respect to laser power, plots of atomic percentage versus laser power is shown in Fig 50. By observing the plots, we can notice that the quantities of Zn and O are relatively constant, as compared to quantity of C. Carbon, on the other hand, seems to be decreasing as the laser power increases. This result is in agreement with the Raman results, providing further support to our argument of carbon-related deep levels. Notice no significant change happens at power beyond 100 mW. This suggests that 100 mW is another critical power which allows the complete oxidation of carbon at the region of interest. The reason of reaching such equilibrium may be due to the disintegration of nano-structures due to high thermal energy (see Fig 45), preventing further reaction to occur.

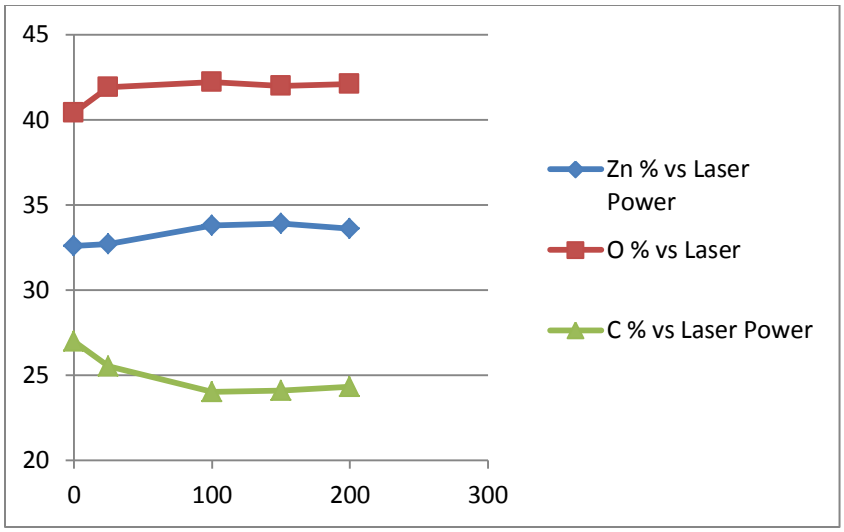

Power (mW)	Zn %	O %	C %
0	32.6	40.4	27
25	32.7	41.9	25.5
100	33.8	42.2	24
150	33.9	42	24.1
200	33.6	42.1	24.3

Fig 50, Top: Plots of the atomic percentage of Zn, O and C versus the power of focused laser beam, Bottom: A table of the data points

References

[1] Haibo Zeng, "Blue Luminescence of ZnO Nanoparticles Based on Non-Equilibrium Process: Defects Origins and Emission Controls", Advanced Functional Materials, 20, pg. 561-572 , (2010)

[2] Chun Li, Liang Huang, Gayatri Pongur Snigdha, Yifei Yu and Linyou Cao, "Role of Boundary Layer Diffusion in Vapor Deposition Growth of Chalcogenide Nanosheets: The Case of GeS", ACS Nano, 2012, 6 (10), pp 8868–887.

[3] K.Y. Lim, K.M. Hew, M.R. Zheng, K.D. Yuan, W. Chen, E.S. Tok, C.H. Sow, "Carbide-enriched ZnO NWs for tunable optical properties"(Manuscript in preparation)

[4] Hong Zhou and Raj N. Singh, “Kinetics Model for the growth of silicon carbide by the reaction of liquid silicon with carbon”, Journal of the American Ceramic Society, 78 [9], 2456-62, 1995.

[5] Doris Segets, Johannes Gradl, Robin Klupp Taylor, Vassil Vassilev, and Wolfgang Peukert, “Analysis of Optical Absorbance Spectra for the Determination of ZnO Nanoparticle Size Distribution, Solubility, and Surface Energy”, ACS Nano, VOL. 3, NO. 7, pg 1703–1710, 2009.

[6] Junpeng Lu, Xiaodai Lim, Minrui Zheng, Subodh G. Mhaisalkar, and Chorng Haur Sow, “Direct Laser Pruning of CdSxSe1-x Nanobelts en Route to a Multicolored Pattern with Controlled Functionalities”, ACS Nano, vol 6, NO. 9, 8298-8307, 2012.

[7] Satinder K Shrama, Neelam Saurakhiya, Sumit Barthwal, Rudra Kumar and Ashutosh Sharma, “Tuning of structural, optical, and magneticproperties of ultrathin and thin ZnO nanowire arrays for nano device applications”, Nanoscale Research Letters 2014, 9:122.

[8] R.S. Krishnan, “Raman Spectrum of Diamond”, Nature, No. 3928, Feb 10, 1945, pg 171.

[9] F. Tuinstra and J. L. Koenig, “Raman Spectrum of Graphite”, The Journal of Chemical Physics 53, 1126 (1970).

[10] Yoon Hee Jang and Dong Ha Kim, “Visible light active photocatalysis on block copolymer induced strings of ZnO nanoparticles doped with carbon”, J. Mater. Chem. A, 2013, 1, 898.

[11] A.C. Ferrari, J. Robertson, Phys. Rev. B 61 (2000) 14095.

[12] A.C. Ferrari, J. Robertson, Phys. Rev. B 64 (2001) 075414.

[13] S. T. Tan, X. W. Sun, Z. G. Yu, P. Wu, G. Q. Lo, and D. L. Kwong, “p -type conduction in unintentional carbon-doped ZnO thin films”, Applied Physics Letters 91, 072101 (2007).

Conclusion

In conclusion, this study confirms the manipulation of the composition of the precursor, in particular the mass ratio of ZnO powder to graphite powder, is an effective way in tuning the fluorescence of ZnO NWs sample. This is important especially for violet emission which only appears at certain mass ratios. Besides, position control is also of upmost importance because it determines the dominance of diffusion flux and surface reaction in contributing to the silicon substrate, resulting in sample with different dominant emission. Another crucial factor that affects the fluorescence is the amount of oxygen. Since during synthesis or post-synthesis treatment, a large amount of oxygen can always turn the fluorescence into green, it is suggested oxygen leads to the increment of green-related deep levels between the energy gap of ZnO.

Laser modification can cause two kinds of changes to the ZnO NWs sample: disintegration and fluorescence alteration. In both cases, carbon seems to play a significant role as the determining factor. While the critical amount remains unknown, the existence of carbon which leads to the formation of Zinc Carbide is likely to determine whether a sample can be disintegrated or not, as suggested by XPS. For the part of fluorescence alteration, we observe the drop of carbon's atomic percentage as the laser power increases. We deduce that carbon is oxidized and released during the process. The fact that greening effect is growing with laser power on the other hand suggests that carbon is likely related to yellow-related deep levels, and thus with the decrease of carbon content, the green-related levels become the main deep levels.

Future Works

Since this study is almost purely experimental, one of the improvements is then the incorporation of proper theoretical formulation. This is likely to be done with the use of density function theory (DFT) because DFT is very useful in conducting first principle calculation or developing energy bands diagram which is able to explain the occurrence of different optical transitions.[1,2]

Another unsolved problem in this study is the identification of the type of defect for each kind of emission (fluorescence). Due to time constraint and the availability of instruments, only a few sets of XPS data were obtained. Due to this insufficiency, we are not able to fully investigate and identify the chemical bonds of the samples. This in turn makes us unable to confirm which kind of chemical reaction(s) is (are) involved. In particular, we cannot confidently prove the existence of carbide bonds. The direct solution might rely on more XPS measurements (hopefully after the renovation). An alternative option to study the effect of carbon is the use of other reducing agent during the synthesis. A suitable choice may be carbon monoxide because firstly it does not introduce new element which may complicate the situation, and secondly its gaseous form prevents it to be incorporated into the substrate.

Last but not least, the fact that this project only deals with one kind of laser and produces a single kind of optical modification, which is the greening, implies it is possible to use other kind of laser to produce other kind of optical modification such as browning.

References

[1] Thierry Pauporté, Oleg Lupan, Jie Zhang, Tugba Tugsuz, Ilaria Ciofini, Frédéric Labat, and Bruno Viana, “Low-Temperature Preparation of Ag-Doped ZnO Nanowire Arrays, DFT Study, and Application to Light-Emitting Diode”, ACS Appl. Mater. Interfaces 2015, 7, 11871−11880.

[2] Kin Mun Wong, S. M. Alay-e-Abbas, Yaoguo Fang, A. Shaukat, and Yong Lei, “Spatial distribution of neutral oxygen vacancies on ZnO nanowire surfaces: An investigation combining confocal microscopy and first principles calculations”, J. Appl. Phys. 114, 034901 (2013).

Appendices

[1] ZnO general properties

Molar Mass	81.408 g/mol
Appearance	White
Density	5.606 g/cm^3
*Melting Point	1975 ˚C (decompose)
*Boiling Point	1975 ˚C (decompose)
Direct Band Gap	3.37 eV
Exciton Binding Energy	60 meV
Refractive Index	2.0041
Crystal Structure (common)	Wurtzite
Lattice Constant	$a = 3.25$ Å , $c = 5.2$ Å
Std. molar entropy (298 K)	43.9 JK^{-1}mol^{-1}
Std. enthalpy of formation (298K)	-348.0 kJ/mol

*cf. The melting point and boiling point of zinc 419.53 ˚C and 907 ˚C respectively. Thus, the synthesis can be conducted in a lower temperature if we reduce ZnO powder to Zn.

[2] Optimized parameters for ZnO NW synthesis

Sputtering

Pressure: $(1.0 \pm 0.1) \times 10^{-3}\ torr$

Duration: 25 minutes

Temperature: 520 ˚C

Power: 100 W

Average thickness of the sputtered layer: 200 nm

CVD

Pressure: $(2.0 \pm 0.1)\ mbar$ (remains constant throughout this study)

Synthesis duration: 5 hours (Dwelling time)

Temperature: 850 ˚C to 900 ˚C (Manipulating variable)

Flow rate of carrier gas: 100 sccm to 110 sccm

Source material: 0.4g mixture of ZnO powder and Graphite powder

Test Tube diameter: 1.6 cm

Test Tube length: 30 cm

[3] Range of different radiations